Theses and Dissertations | 1. Thesis and Dissertation Collection, all items

1990-09

On the use of sympathetic resonators to improve low frequency transducer performance

Ellsworth, John Merle

Monterey, California: Naval Postgraduate School

http://hdl.handle.net/10945/34886

AD-A241 349

NAVAL POSTGRADUATE SCHOOL
Monterey , California

DTIC
ELECTE
OCT 0 8 1991
S B D

THESIS

ON THE USE OF SYMPATHETIC
RESONATORS TO IMPROVE LOW
FREQUENCY TRANSDUCER PERFORMANCE

by

John Merle Ellsworth

September 1990

Advisor: S. R. Baker
Second Reader: O. B. Wilson

Approved for public release; distribution unlimited.

91-12569

REPORT DOCUMENTATION PAGE		Form Approved OMB No 0704-0188

1a REPORT SECURITY CLASSIFICATION UNCLASSIFIED	1b RESTRICTIVE MARKINGS
2a SECURITY CLASSIFICATION AUTHORITY	3 DISTRIBUTION/AVAILABILITY OF REPORT
2b DECLASSIFICATION/DOWNGRADING SCHEDULE	Approved for public release; distribution is unlimited.

4 PERFORMING ORGANIZATION REPORT NUMBER(S)	5 MONITORING ORGANIZATION REPORT NUMBER(S)

6a NAME OF PERFORMING ORGANIZATION Naval Postgraduate School	6b OFFICE SYMBOL (If applicable) 3A	7a NAME OF MONITORING ORGANIZATION Naval Postgraduate School
6c. ADDRESS (City, State, and ZIP Code) Monterey, CA 93943-5000		7b ADDRESS (City, State, and ZIP Code) Monterey, CA 93943-5000

8a NAME OF FUNDING/SPONSORING ORGANIZATION	8b OFFICE SYMBOL (If applicable)	9 PROCUREMENT INSTRUMENT IDENTIFICATION NUMBER

8c ADDRESS (City, State, and ZIP Code)	10 SOURCE OF FUNDING NUMBERS			
	PROGRAM ELEMENT NO	PROJECT NO	TASK NO	WORK UNIT ACCESSION NO

11 TITLE (Include Security Classification)

On the Use of Sympathetic Resonators To Improve Low Frequency Transducer Performance (Unclassified)

12 PERSONAL AUTHOR(S) Ellsworth, John Merle

13a TYPE OF REPORT Master's Thesis	13b TIME COVERED FROM _____ TO _____	14 DATE OF REPORT (Year, Month, Day) 1990 September	15 PAGE COUNT 70

16 SUPPLEMENTARY NOTATION

The views expressed in this thesis are those of the author and do not reflect the official policy or position of the Department of Defense or the U.S. Government.

17	COSATI CODES		18 SUBJECT TERMS (Continue on reverse if necessary and identify by block number)
FIELD	GROUP	SUB-GROUP	Low Frequency Active, Multiple Scatter, Sympathetic Resonance, Quasiresonance, Coupled Network Analysis

19 ABSTRACT (Continue on reverse if necessary and identify by block number)

The achievable gain in the radiation resistance and directivity of a low frequency underwater transducer due to the presence of an array of sympathetic resonators was analyzed. The resonators were all taken to be air bubbles, and both the resonators and transducer were taken to be compact $(ka \ll 1)$. The resonators were taken to be equally spaced around a circle of radius R, with the transducer located on the axis. The gain was calculated for various numbers of resonators as a function of $ka_{resonator}$, $ka_{transducer}$ and kR, for the transducer in the plane of the resonators and

20 DISTRIBUTION/AVAILABILITY OF ABSTRACT ☒ UNCLASSIFIED/UNLIMITED ☐ SAME AS RPT ☐ DTIC USERS	21 ABSTRACT SECURITY CLASSIFICATION
22a NAME OF RESPONSIBLE INDIVIDUAL Steven R. Baker	22b TELEPHONE (Include Area Code) (408) 646 2732	22c OFFICE SYMBOL PH/BA

DD Form 1473, JUN 86 Previous editions are obsolete SECURITY CLASSIFICATION OF THIS PAGE

S/N 0102-LF-014-6603

out of the plane one-quarter wavelength. For the transducer in the plane, a gain in radiation resistance of approximately two is possible with six or more resonators. For the transducer out of the plane, it is shown that a significant gain in directivity can be achieved at the expense of a slight decrease in the gain in the radiation resistance.

Accession For

NTIS GRA&I	☑
DTIC TAB	☐
Unannounced	☐
Justification	

By
Distribution/
Availability Codes

| Dist | Avail and/or Special |
| A-1 | |

COPY
INSPECTED
4

On The Use Of Sympathetic Resonators To Improve Low Frequency
Transducer Performance

by

John Merle Ellsworth
Lieutenant , United States Navy
B. E., State University of New York, Stony Brook, 1980

Submitted in partial fulfillment of the
requirements for the degrees of

MASTER OF SCIENCE IN ENGINEERING ACOUSTICS

and

MASTER OF SCIENCE IN APPLIED SCIENCE

(Antisubmarine Warfare) ·

from the

NAVAL POSTGRADUATE SCHOOL

September 1990

Author: _____

(John Merle Ellsworth

Approved by: _____

Steven R. Baker, Advisor

_____

Oscar B. Wilson, Second Reader

_____

Anthony A. Atchley, Chairman
Engineering Acoustics Academic Committee

_____

Robert N. Forrest , Chairman
Antisubmarine Warfare Academic Group

ABSTRACT

The achievable gain in the radiation resistance and directivity of a low frequency underwater transducer due to the presence of an array of sympathetic resonators was analyzed. The resonators were all taken to be air bubbles, and both the resonators and transducer were taken to be compact ($ka \ll 1$). The resonators were taken to be equally spaced around a circle of radius R, with the transducer located on the axis. The gain was calculated for various numbers of resonators as a function of $ka_{resonator}$, $ka_{transducer}$ and kR, for the transducer in the plane of the resonators and out of the plane a distance of one-quarter wavelength. For the transducer in the plane, a gain in radiation resistance of approximately two is possible with six or more resonators. For the transducer out of the plane, it is shown that a significant gain in directivity can be achieved at the expense of a slight decrease in the gain in the radiation resistance.

THESIS DISCLAIMER

The views expressed in this thesis are those of the author and do not reflect the official policy of or position of the Department of Defense or the U.S. Government.

The reader is cautioned that computer programs developed in this research may not have been excerised for all cases of interest. While every effort has been made, within the time available, to ensure that the programs are free of computational and logic errors, they cannot be considered validated. Any application of these programs without additional verification is at the risk of the user.

TABLE OF CONTENTS

ACKNOWLEDGEMENTS

LIST OF SYMBOLS

a_n Radius of element n.

c Speed of sound in water.

G_R The ratio of the acoustic radiation resistance of a transducer with sympathetic resonators present to the acoustic radiation resistance of an identical transducer with no resonators.

k Wave number, ω/c.

ka_1 The resonance value of ka for a single air filled bubble.

l_{nm} Separation distance between element n and m.

p_n^f Incident free field acoustic pressure at element n due to external field only.

p_n Surface pressure at element n.

p_n^{sc} Scattered pressure at the surface of resonator n, in the presence of other resonators.

P_{single}^{sc} Scattered pressure at the surface of a single resonator. i.e. in the absence of other resonators.

$\dot{q}$ Mass injection rate of a spherical sound source.

r Distance from scatterer center to a field point.

z Specific acoustic impedance, pressure divided by surface normal velocity.

A Single scatter amplification coefficient of element n.

B Multiple scatter amplification coefficient of element n.

C_{nm} Ratio of acoustic impedances defined as:

$$C_{nm} = \frac{Z_{nm}^{ar}}{Z_{mm}^{ar}}$$

D_n Ratio of acoustic impedances, defined as:

$$D_n = -\frac{Z_{nn}^{ar} + Z_n^a}{Z_{nn}^{ar}}$$

$\mathcal{F}_a$ Scattered acoustic pressure from a single scatterer, normalized to the incident acoustic field.

$\mathcal{F}_b$ Scattered acoustic pressure from a scatterer, interacting with other scatterers, normalized to the incident acoustic field

I Electrical current.

P_0 Ambient pressure of environment.

S_n Surface area of element n.

T Transduction coefficient.

U_n Volume velocity of element n.

U_n^{rel} Volume velocity of element n, normalized to transducer's volume velocity.

V Volume of source.

Z Acoustic impedance, pressure divided bvolume velocity.

Z_n^a Acoustic impedance of element n.

Z_{nn}^{ar} Acoustic radiation impedance seen by element n with all other elements blocked.

Z_{nm}^{ar} Acoustic transfer impedance from element m to element n.

Z_{total}^{ar} The total acoustic radiation impedance seen by transducer in the presence of sympathetic resonators.

Z^{ao} Transducer open circuit (I=0) acoustical impedance.

δ_{nm} Kronecker delta function, where:

$$\delta_{nm} = \left\{ \begin{array}{l} 1;\ m=n \\ 0;\ m\neq n \end{array} \right\}$$

ρ Density of water.

μ Ratio of the magnitudes of the scattered acoustic pressure at the surface of a resonant scatterer to the incident acoustic pressure in the presence of other scatterers.

μ_0 Ratio of the magnitudes of the scattered acoustic pressure at the surface of a single resonant scattererto the incident acoustic pressure.

γ Ratio of specific heats (air).

ω Angular frequency of plane wave.

ω_0 Angular frequency of scatterer resonance.

ζ Defined as:

$$\zeta = \frac{(\omega_0^2/\omega^2 - 1)}{ka}$$

$\{X_n\}$ A Nx1 column matrix, n = 1...N.

X_{nm} A NxN square matrix, n,m = 1...N.

(This page intentionaly left blank.)

I. INTRODUCTION

A. BACKGROUND AND HISTORY

I. Tolstoy [Ref. 1],[Ref 2] and A. Tolstoy and I. Tolstoy [Ref. 3] have recently analyzed the multiple scattering of sound from a collection of compact (ka<<1) monopole scatterers (e.g. gas filled bubbles, gas filled balloons and thin shells in water) insonified by a simple harmonic plane wave at frequencies close to the resonance frequency of an individual scatterer. The response of these systems was quantified by computing the ratio of the scattered pressure on the surface of a scatterer in the presence of the other elements to that of the incident plane wave. This ratio was defined as the amplification factor, μ. They investigated the value of this amplification factor for various simple geometrical arrangements of monopole resonant scatterers, and showed that amplification factors of the order of 10^2 were to be expected for air bubbles in water at one atmosphere ambient pressure. (The amplification factor of a single bubble is about 70.) These systems were said to be "quasiresonant".

I. Tolstoy [Ref. 4] has also recently analyzed the strength and directionality of the resonant multiple scattering of sound from a linear array of compact monopole resonant scatterers irradiated by a plane wave. He reports that "quasiresonance" effects exhibit strong directionality in this system, with amplification factors of up to 700. The potential application of resonant multiple scattering, or "quasiresonance", in Tolstoy's words, to improve the performance of a

1

low frequency active sonar transducer is the subject of the research described in this thesis.

B. OBJECTIVES

The objectives of this research are multiple. The first is to reproduce I. Tolstoy's results using network analysis, a tool familiar to the transducer and array designer. It will then be shown that the two methods of analysis, multiple scattering and network analysis, give identical results. The existence of quasiresonance will then applied to a circular array of scatterers, where the incident plane wave is replaced by an active transducer located on the axis of the circle and radiating spherical waves. The acoustic advantage gained in this system will be quantified by the gain in the radiation resistance seen by the transducer in the presence of these scatterers. An increase in radiation resistance enables the transfer of more power to the acoustic field for a given surface velocity of the transducer. (High power low frequency active sonar transducers tend to be resonant devices that are displacement limited.) The cases of the transducer in the plane of the circle and displaced by one-quarter wavelength from the plane will be analyzed for both their increase in radiation resistance and gain in directivity over that of a single transducer.

2

II. THEORY

A. QUASIRESONANCE

For simple configurations of compact resonant scatterers insonified by a simple harmonic plane wave, Tolstoy predicted the existence of so-called "quasiresonance" using multiple scattering theory. (Quasiresonance is Tolstoy's term for the enhancement of the scattered pressure from a resonant scatterer as a result of multiple scattering.) Tolstoy's analysis will be reviewed and applied to the simplest case in section A1. In section A2 the same problem is treated using network analysis. The existence of quasiresonance is again predicted using a coupled network model. It will be shown that this second method produces results identical to Tolstoy's.

1. TOLSTOY'S ANALYSIS OF MULTIPLE SCATTER

Tolstoy's analysis of the multiple scattering of a plane wave incident upon a collection of compact resonant scatterers proceeds using linear theory of acoustics. The following development parallels that of Reference [1] and Reference [3], with the difference being that here all time-harmonic functions are taken to be of the form $e^{j\omega t}$. This will result in minor differences in the appearance of otherwise equivalent equations.

Consider first the case of a single resonant scatterer insonified by an incident plane wave. From Lighthill [Ref. 5], the sound field of a spherical source is given by Equation 2-1.

3

$$p(r,t) = (4\pi r)^{-1} \dot{q}(t-r/c)$$

(2-1)

where:

r = Distance from scatterer center to the field point.
q = Mass injection rate of a spherical sound source.
c = Speed of sound in water.

The dot over q indicates the derivative with respect to time. Treating the single scatterer as an air filled bubble, for an incident plane wave of free field pressure p^f, $\dot{q}$ takes the form of Equation 2-2.

$$\dot{q} = p^f k^2 V \left(\frac{\gamma P_0}{\rho c^2} - 1\right)\left(1 - (1-jka)\frac{\omega^2}{\omega_0^2}\right)e^{j\omega t}$$

(2-2)

where:

p^f = Incident free field acoustic pressure.
k = Wave number, ω/c.
V = Volume of scatterer.
a = Scatterer radius.
γ = Ratio of specific heats (air).
c = Speed of sound in water.
ρ = Density of water.
P_0 = Ambient pressure of environment.
ω = Angular frequency of plane wave.
ω_0 = Resonance frequency of scatterer.

Inserting Equation 2-2 into Equation 2-1, dropping the time dependence, and solving for the ratio of the scattered acoustic pressure at some radius r from the scatterer, $p^{sc}_{single}(r)$, to that of the incident pressure, p^f, one obtains Equation 2-3.

$$\frac{p^{sc}_{single}(r)}{p^f} = \frac{1}{jkr}\left(\frac{1}{1-j\zeta}\right)e^{-jkr}$$

(2-3)

4

where:

$$\zeta = \frac{\left(\omega_0^2/\omega^2 - 1\right)}{ka}$$

For situations where the surface tension and corrections due to energy losses in the interior of the scatterer (e.g. bubbles, balloons) are negligible, the ratio of the resonance angular frequency of the scatterer to the angular frequency of the incident plane wave is given by Equation 2-4.

$$\frac{\omega_0}{\omega} = \sqrt{\frac{3\gamma P_0}{\rho c^2 (ka)^2}} \tag{2-4}$$

Letting r equal a, the scatterer radius in Equation 2-3, results in Equation 2-5, the ratio of the scattered acoustic pressure at the single scatterer's surface to that of the incident free field pressure.

$$\frac{p_{single}^{sc}}{p^f} = \frac{1}{jka} \left(\frac{1}{1-j\zeta}\right) e^{-jka} \tag{2-5}$$

Tolstoy introduces the quantities $\mathcal{F}_a$ and A by rewriting Equation 2-3 as Equation 2-6.

$$\mathcal{F}_a = \frac{p_{single}^{sc}(r)}{p^f} = A\frac{e^{-jkr}}{jkr} \tag{2-6}$$

where:

$$A = \frac{1}{1-j\zeta}$$

F_a is the normalized scattered acoustic pressure for a single scatterer insonified by an incident plane wave and A is the single-scatterer amplitude coefficient.

Now consider a system of N identical interacting scatterers insonified by a plane wave. Let $p_n^{sc}(r)$ represent the scattered acoustic pressure. An equation for $p_n^{sc}(r)/p_n^f$, equivalent to that of Equation 2-6 for a single scatterer, can be written as Equation 2-7 for the multiple scatterer situation.

$$F_{b_n} = \frac{p_n^{sc}(r)}{p_n^f} = B_n \frac{e^{-jkr}}{jkr}$$

(2-7)

F_{b_n} is the normalized scattered acoustic pressure from scatterer n, insonified by both the incident plane wave and the fields of the other scatterers, p_n^f is the free field pressure of the incident plane wave at scatterer n, and B_n is the multiple scatterer amplitude coefficient for scatterer n.

For compact scatterers, the overall response of a scatterer to multiple incident pressure fields can be evaluated by summing up the response to each individual incident pressure field [Ref. 3]. For a system of N scatterers, this results in Equation 2-8 for the scattered field at the surface of the nth resonator.

$$B_n \frac{e^{-jka_n}}{jka_n} = A_n \left(1 + \sum_{m \neq n} B_m \frac{e^{-jkl_{nm}}}{jkl_{nm}} e^{j\psi_{nm}} \right) \frac{e^{-jka_n}}{jka_n}$$

(2-8)

where: Ψ_{nm} is the phase difference in the incident plane wave between resonator m and n, and m=1...N. The subscript notation for A has been added to allow for a system of different sized scatterers.

Tolstoy defines the amplification factor μ (different than the scatter amplitude coefficient mentioned previously) to be the magnitude of the ratio of the scattered acoustic pressure on the surface of a scatterer, p_n^{sc}, to the incident free field acoustic pressure of the incident plane wave, p_n^f. With this definition, Equation 2-9 follows from Equation 2-7.

$$\mu_n = \left|\frac{p_n^{sc}}{p_n^f}\right| \approx \frac{|B_n|}{ka_n} \tag{2-9}$$

Tolstoy denotes the amplification factor for a single scatterer as μ_0. Equation 2-10, then, follows from Equation 2-6.

$$\mu_{0_n} = \left|\frac{p_{single_n}^{sc}}{p_n^f}\right| = \frac{|A_n|}{ka_n} \tag{2-10}$$

From Equations 2-9 and 2-10, μ/μ_0 is expressed in terms of B_n/A_n by Equation 2-11.

$$\frac{\mu_n}{\mu_{0_n}} = \left|\frac{p_n^{sc}}{p_{single_n}^{sc}}\right| = |B_n/A_n| \tag{2-11}$$

a. APPLICATION OF TOLSTOY'S METHOD

As an example application, Tolstoy considered a system of two identical resonators insonified by a plane wave traveling along the axis joining their centers, as shown in Figure 2-1.
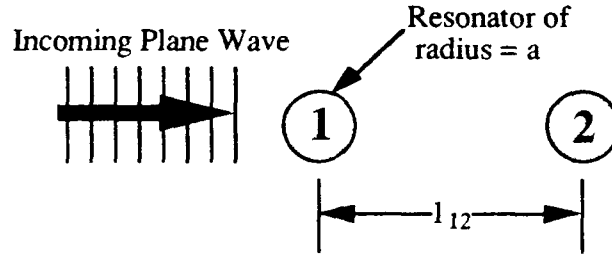
7

Figure 2-1. A Two Resonator System Insonified by
a Plane Wave Along the Axis of The Resonators.

Application of Equation 2-8 to the situation shown in Figure 2-1
results in the set of Equations 2-12.

$$B_1 \frac{e^{-jka}}{jka} = A\frac{e^{-jka}}{jka} + A \frac{e^{-jka}}{jka} B_2 \frac{e^{-jkl}}{jkl} e^{-jkl}$$

$$B_2 \frac{e^{-jka}}{jka} = A\frac{e^{-jka}}{jka} + A \frac{e^{-jka}}{jka} B_1 \frac{e^{-jkl}}{jkl} e^{jkl}$$

(2-12)

For a system of identical scatterers, the values of A_1 and A_2 are equal.
Therefore, the subscript on A in Equation 2-12 has been omitted.
Since all variables in Equation 2-12 are known except B_1 and B_2, one
can solve for B_1/A in terms of A and kl, resulting in Equation 2-13.

$$B_1/A = \frac{1 + \left(A \frac{e^{-jkl}}{jkl} \right) e^{-jkl}}{1 - \left(A \frac{e^{-jkl}}{jkl} \right)^2}$$

(2-13)

Substituting the expressions for ζ and ω/ω_0 for an air-filled bubble into
the expression for A, B_1/A is given in terms of the variables ka, kl, c,
P_0, and ρ by Equation 2-14.

8

$$B_1/A = \frac{p_1^{sc}}{p_{single}^{sc}} = \frac{1 - e^{-jkl}\left(\dfrac{\dfrac{ka}{kl}e^{j(ka-kl)}}{\rho c\left((ka)^2+j\left(ka - \dfrac{3\gamma P_0}{\rho c^2(ka)}\right)\right)}\right)}{1 - \left(\dfrac{\dfrac{ka}{kl}e^{j(ka-kl)}}{\rho c\left((ka)^2+j\left(ka - \dfrac{3\gamma P_0}{\rho c^2(ka)}\right)\right)}\right)^2} \tag{2-14}$$

For bubbles just under the surface of the ocean, we take:

P_0 = 10132 Pa (1 atmosphere)

ρ = 998 kgm^{-3}

c = 1498 ms^{-1}

As observed by Tolstoy [Ref. 3], plots of Equation 2-14 display spurious peaks. Following Tolstoy, then, the graphs of $|B_1/A|$ versus ka and kl, plotted in Figures 2-2a,b have been treated to limit peaks in bound intervals less than 2ka. (According to Tolstoy peaks narrower than 2ka, where 2a equals the resonator diameter, are not meaningful, since the pressure over a compact resonator is approximately constant.) The truncation method used involved comparing three consecutive values of $|B_1/A|$ in the kl direction for each value of ka. (Three consecutive points in the kl-direction span approximately 2ka.) If the value of $|B_1/A|$ for the middle point was greater than either of its neighboring points (a peak) then this value was set equal to the mean of the two neighboring points. This procedure was repeated several times to get the desired smoothing.

9
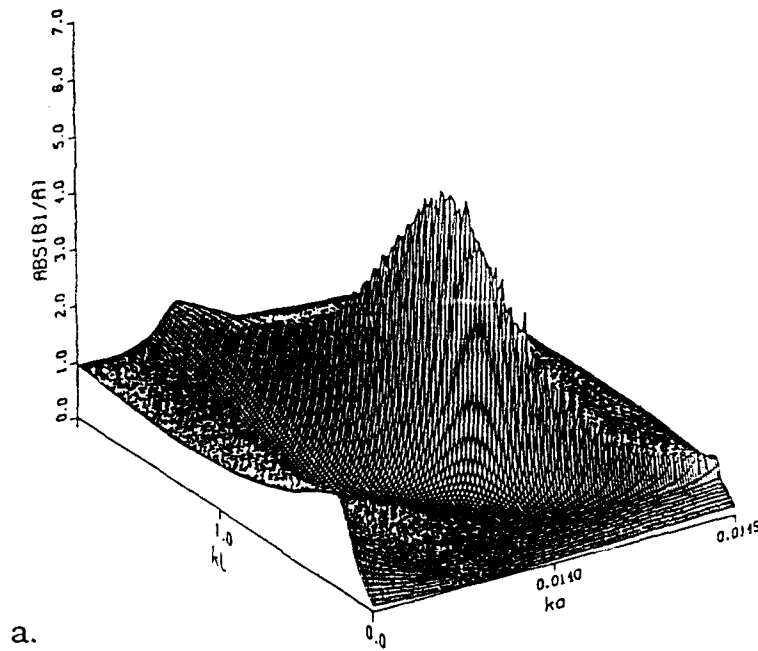
a.
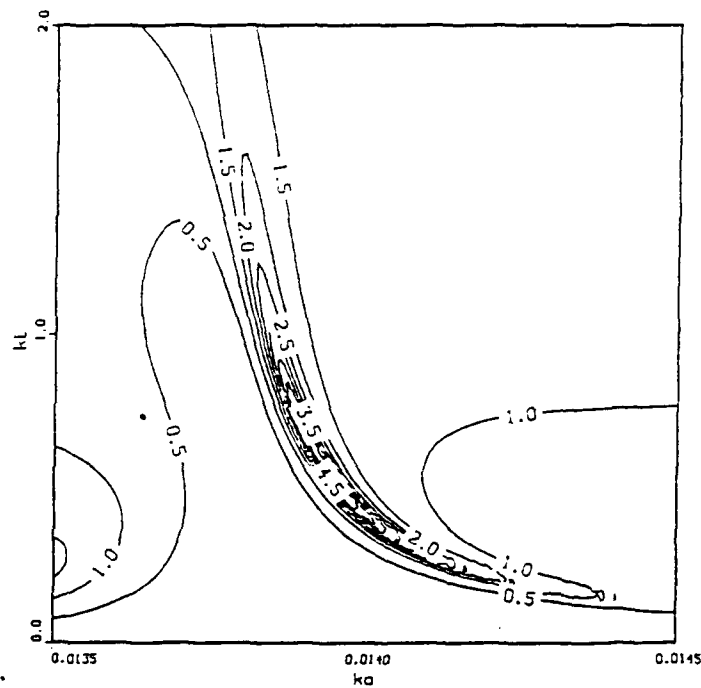
b.

Fig. 2-2a,b.   Three Dimensional (a), and Contour (b) Plots Showing
$|B_1/A|$ for the Double Resonator   System as a Function of ka and
kl for Axial Incidence of the Plane Wave.

10

Figures 2-2a,b show a maximum response of $|B_1/A|$ equal to 5.5 at approximately ka=0.01393 and kl=0.60. As a result of multiple scattering, then, the scattered pressure amplitude of the first bubble is 5.5 times greater in the presence of the second bubble than in its absence. Additionally, the value of ka at the maximum response is shifted from that for a single resonant bubble of .01379.

2. NETWORK ANALYSIS OF MULTIPLE SCATTER

Fig. 2-3 displays a network model of N interacting scatterers insonified by an incident acoustic wave. (Note: pressure (p) and volume velocity (U_n) are chosen as the mechanical variables, and the direction of positive velocity is clockwise.) The network equations for Fig. 2-3 are:

$$p_n = p_n^f + \sum_{m=1}^{N} Z_{nm}^{ar} U_m \qquad p_n = -Z_n^a U_n \qquad (2\text{-}15)$$

where for Fig 2-3:

$p_n=$ Surface pressure at element n.

$p_n^f=$ Free field pressure at element n due to an externally incident field only.

$U_n=$ Volume velocity of element n.

$Z_n^a=$ Acoustic impedance of element n.

$Z_{nn}^{ar}=$ Acoustic radiation impedance seen by element n with all other elements blocked. ($U_{m \neq n} = 0$ m=1...N)

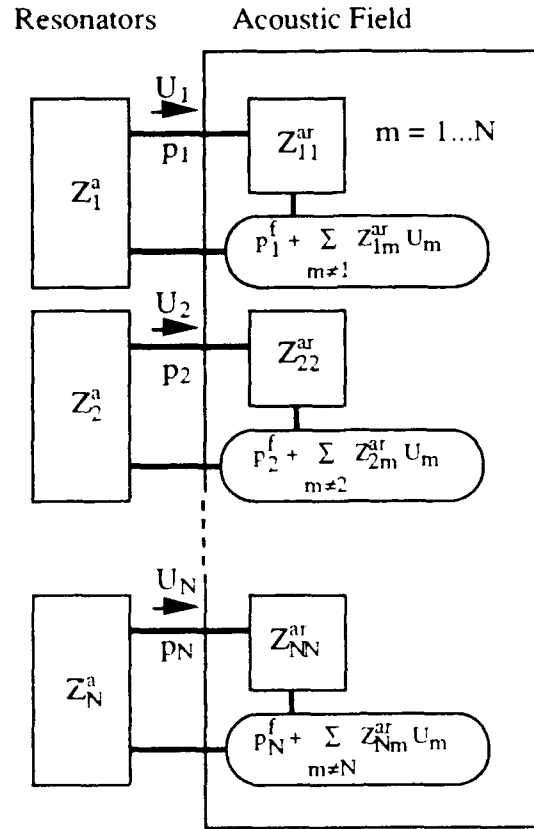$Z_{n,m}^{ar}=$ Acoustic transfer impedance from element m to element n.

Figure 2-3. Network Model of N Interacting Resonators Insonified by a Plane wave.

Neglecting the effects of surface tension, thermal relaxation, etc., the intrinsic acoustic impedance of a small ($ka<<1$) gas-filled bubble can be approximated by one of reactance only, given by Kinsler, Frey, Coppens and Sanders [Ref. 6] as Equation 2-16.

$$Z_n^a = j \frac{-3\gamma P_0}{c(ka_n)} S_n^{-1}$$

(2-16)

where:

a_n = Radius of element n.
c = Speed of sound in water.
k = Wave number, ω/c.
P_0 = Ambient pressure of environment.

12

S_n = Surface area of element n.

γ = Ratio of specific heats (air).

The self acoustic radiation impedance seen by element n, Z_{nn}^{ar}, can be approximated by Equation 2-17.

$$Z_{nn}^{ar} = \rho c \left((ka_n)^2 + jka_n \right) S_n^{-1}$$
(2-17)

where:

ρ = density of water.

Equation 2-17 is the acoustic radiation impedance presented to a compact source with no other active or scattering elements present. It is also the acoustic radiation impedance seen by a compact source in the presence of other compact sources when these sources are blocked $(U_{m \neq n} = 0 \quad m = 1...N)$.

The acoustic transfer impedance from element m to element n is given by Equation 2-18.

$$Z_{nm}^{ar} = Z_{mm}^{ar} \frac{ka_m}{kl_{nm}} e^{j(ka_m - kl_{nm})}$$
(2-18)

In matrix form the network equations (Equation 2-15) can be written as Equation 2-19.

$$\{p_n\} = \left[Z_{nm}^{ar} \right] \{U_m\} + \{p_n^f\} \quad m,n = 1...N$$
(2-19)

where:

$\{X_n\}$ n = 1...N   A 1xN column matrix, N elements.

$\lceil X_{nm} \rceil$ n,m = 1...N   A NxN square matrix, N^2 elements.

Substituting $p_n = -Z_n^a U_n$ and rearranging results in Equation 2-20.

13

$$\{-p_n^f\} = \left[Z_{nm}^{ar} + Z_n^a \delta_{nm}\right]\{U_m\} \quad m,n = 1...N \tag{2-20}$$

where

δ_{nm} = Kronecker delta function,

$$\delta_{nm} = \left\{ \begin{array}{l} 1;\ m=n \\ 0;\ m\neq n \end{array} \right\}.$$

a. APPLICATION OF NETWORK ANALYSIS

Modeling the system of two scatterers shown in Figure 2-1 as a network, Equation 2-20 becomes Equation 2-21.

$$\left| \begin{array}{c} -p_1^f \\ -p_2^f \end{array} \right| = \left| \begin{array}{cc} Z_{11}^{ar} + Z_1^a & Z_{12}^{ar} \\ Z_{21}^{ar} & Z_{22}^{ar} + Z_2^a \end{array} \right| \left| \begin{array}{c} U_1 \\ U_2 \end{array} \right| \tag{2-21}$$

Using the relation $p_n^{sc} = Z_{nn}^{ar}U_n$ to eliminate U_n, the above equations can be written in terms of the scattered acoustic pressure at each individual resonator, p_n^{sc}, and the incident plane wave pressures as given by Equation 2-22.

$$p_1^{sc} = \left(p_1^f + C_{12}\, p_2^{sc}\right) D_1^{-1}$$
$$p_2^{sc} = \left(p_2^f + C_{21}\, p_1^{sc}\right) D_2^{-1} \tag{2-22}$$

where

$$C_{nm} = \frac{Z_{nm}^{ar}}{Z_{mm}^{ar}} \qquad D_n = -\frac{Z_{nn}^{ar} + Z_n^a}{Z_{nn}^{ar}}$$

For a system of identical resonators, C_{nm} and D_n are the same for all m and n; therefore the subscript notation is not required. Solving Equation 2-22 for the scattered acoustic pressure at each resonator in

14

terms of the incident plane wave pressure results in Equation 2-23 for the scattered pressure at resonator one.

$$p_1^{sc} = \frac{p_1^f D + p_2^f C}{D^2 - C^2}$$

(2-23)

The scattered acoustic pressure at the first resonator in the absence of the second resonator, $p_{single_1}^{sc}$, is obtained using Equation 2-23 by letting the transfer coefficient C equal zero, resulting in Equation 2-24.

$$p_{single_1}^{sc} = \frac{p_1^f}{D}.$$

(2-24)

Dividing equation Equation 2-23 by 2-24 results in Equation 2-25 for the ratio B_1/A as defined by Tolstoy.

$$B_1/A = \frac{p_1^{sc}}{p_{single_1}^{sc}} = \frac{1 + (p_2^f/p_1^f)\left(\frac{C}{D}\right)}{1 - \left(\frac{C}{D}\right)^2}$$

(2-25)

Inserting Equations 2-16 thru 2-18 into Equation 2-25, one obtains an equation for B_1/A in terms of the variables ka, kl, c, P_0, p_1^f, p_2^f and ρ as given by Equation 2-26.

$$B_1/A = \frac{p_1^{sc}}{p_{single\,1}^{sc}} = \frac{1 - \left(p_2^f/p_1^f\right)\left(\dfrac{\frac{ka}{kl}e^{j(ka-kl)}}{\rho c\left((ka)^2 + j\left(ka - \dfrac{3\gamma P_0}{\rho c^2(ka)}\right)\right)}\right)}{1 - \left(\dfrac{\frac{ka}{kl}e^{j(ka-kl)}}{\rho c\left((ka)^2 + j\left(ka - \dfrac{3\gamma P_0}{\rho c^2(ka)}\right)\right)}\right)^2} \qquad (2\text{-}26)$$

The incident plane wave pressures p_1^f and p_2^f are of equal magnitude and differ only by the phase factor $e^{jkl_{12}}$, resulting in Equation 2-27.

$$\frac{p_2^f}{p_1^f} = e^{-jkl} \qquad (2\text{-}27)$$

Substituting this expression into Equation 2-26, one obtains Equation 2-28.

$$B_1/A = \frac{p_1^{sc}}{p_{single\,1}^{sc}} = \frac{1 - e^{-jkl}\left(\dfrac{\frac{ka}{kl}e^{j(ka-kl)}}{\rho c\left((ka)^2 + j\left(ka - \dfrac{3\gamma P_0}{\rho c^2(ka)}\right)\right)}\right)}{1 - \left(\dfrac{\frac{ka}{kl}e^{j(ka-kl)}}{\rho c\left((ka)^2 + j\left(ka - \dfrac{3\gamma P_0}{\rho c^2(ka)}\right)\right)}\right)^2} \qquad (2\text{-}28)$$

Equation 2-28 is identical to Equation 2-14, demonstrating the equivalence of Tolstoy's method and the network analysis method.

3. A TRANSDUCER IN A MULTI-RESONATOR FIELD

Network analysis will now be applied to the problem of a compact transducer in the presence of an array of interacting, compact resonant scatterers. The procedure is the same here as in section A2,

except that the incident plane wave is replaced by an outward traveling spherical wave whose source is a compact transducer. A network model of the transducer and N resonator system is shown in Figure 2-4.
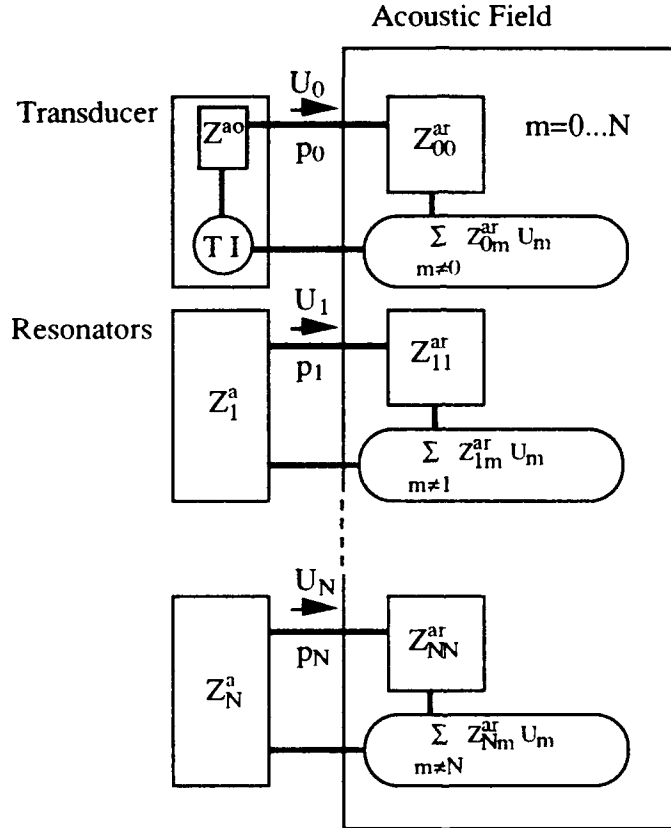
Acoustic Field

Fig. 2-4. Network Model of a Single Transducer and an N Resonator Field.

The network equations for Fig. 2-4 are;

$$p_n = \sum_m Z^{ar}_{nm} U_m \qquad p_n = -Z^a_n\, U_n \quad \text{for } n = 1...N \qquad p_0 = TI - Z^{ao}\, U_0 \qquad (2\text{-}29)$$

where

T = transduction coefficient.

Z^{ao} = transducer open circuit (I=0) acoustic impedance.

17

and the subscript n=0 denotes the transducer, n≠0 a resonator.

The transducer's open circuit acoustic impedance (Z^{ao}) and transduction coefficient (T) are shown only for completeness and will not be considered further, as the quantity of interest will be the radiation impedance presented to the transducer.

Using the network Equations 2-29, the matrix equation for the network model shown in Figure 2-4 is given by Equation 2-30.

$$\left|\begin{array}{c} p_0 \\ \{p_n\} \end{array}\right| = \left|\begin{array}{cc} Z^{ar}_{00} & \{Z^{ar}_{m0}\}^T \\ \{Z^{ar}_{n0}\} & [Z^{ar}_{nm}] \end{array}\right| \left|\begin{array}{c} U_0 \\ \{U_m\} \end{array}\right| ; \quad n, m = 1...N$$

(2-30)

where

$\{X_{n0}\}$ n=1...N   denotes a 1xN column matrix, N elements.

$[X_{nm}]$ n,m=1...N   denotes a NxN square matrix, N^2 elements.

and the superscript T denotes transpose. Replacing the 1 x N surface pressure matrix, $\{p_n\}$, with $\{-Z^a_n U_n\}$ and then normalizing by U_0, the transducer's volume velocity, Equation 2-30 becomes Equation 2-31.

$$\left|\begin{array}{c} Z^{ar}_{total} \\ \{0\} \end{array}\right| = \left|\begin{array}{cc} Z^{ar}_{00} & \{Z^{ar}_{m0}\}^T \\ \{Z^{ar}_{n0}\} & [Z^{ar}_{nm} + Z^a_n \delta_{nm}] \end{array}\right| \left|\begin{array}{c} 1 \\ \{U^{rel}_m\} \end{array}\right| ; \quad n, m = 1...N$$

(2-31)

where

Z^{ar}_{total} = Total acoustic radiation impedance seen by the transducer.

U^{rel}_m = Ratio of element m's volume velocity to that of the transducer $(U^{rel}_m = U_m/U_0)$.

Equation 2-31 can be written as two separate matrix equations, Equations 2-32a,b.

$$Z_{total}^{ar} = Z_{00}^{ar} + \{Z_{m0}^{ar}\}^{T} \{U_{m}^{rel}\}$$ (2-32a)

$$\{0\} = \{Z_{n0}^{ar}\} + [Z_{nm}^{ar} + Z_{n}^{a}\delta_{nm}]\{U_{m}^{rel}\}$$ (2-32b)

Solving Equation 2-32b for $\{U_{m}^{rel}\}$ by matrix inversion and substituting the result into Equation 2-32a, one obtains Equation 2-33, the total acoustic radiation impedance seen by the transducer.

$$Z_{total}^{ar} = Z_{00}^{ar} - \{Z_{m0}^{ar}\}^{T} [Z_{nm}^{ar} + Z_{n}^{a}\delta_{nm}]^{-1} \{Z_{n0}^{ar}\}$$ (2-33)

Equation 2-33 expresses this impedance in terms cf the radiation and transfer impedances of the individual elements.

The tot·l acoustic power radiated by the transducer is given by Equation 2-34.

$$\Pi = \frac{1}{2}| U_{0}|^{2} Re(Z_{total}^{ar})$$ (2-34)

The gain in power delivered to the acoustic field due to the addition of the sympathetic resonators equals the ratio of total power delivered with the resonators present to the power delivered when they are absent, $\Pi = \frac{1}{2}| U_{0}|^{2} Re(Z_{00}^{ar})$. For a displacement-limited source, typical of a sonar projector operated near its resonant frequency, this ratio reduces to the ratio of the radiation resistances for the two cases. This gain factor is expressed as Equation 2-35.

$$G_{R} = \frac{Re(Z_{total}^{ar})}{Re(Z_{00}^{ar})}$$ (2-35)

III . ANALYSIS

A. ANALYSIS OF RESONATOR AND TRANSDUCER CONFIGURATIONS

The theory developed in the previous chapter will now be applied to two specific geometric configurations of a transducer and N identical resonators. The resonators will be treated as simple gas filled bubbles. It is assumed throughout that the acoustic wavelength is much larger than the dimensions of the transducer and the resonators. For initial calculations, ambient pressure is taken to be one atmosphere, and the radius of the transducer is taken to be equal to that of the resonators ($ka_0 = ka_n$).

1. PLANAR CONFIGURATION

The geometry of the first arrangement to be analyzed is shown in Figure 3-1. It consists of N identical resonators equally spaced
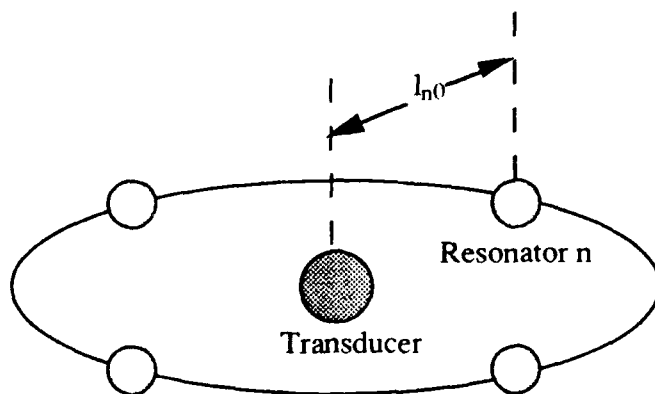
Figure 3-1. Resonators Equally Spaced around Transducer in a Planar Configuration of Radius l_{n0}, N=4.

around a circle of radius l_{n0}. This geometric arrangement will be referred to as the planar configuration.

For the configuration shown in Figure 3-1, Equation 2-35 becomes Equation 3-1.

$$G_R = \frac{Re\left(Z^{ar}_{00} - \{Z^{ar}_{mo}\}^T \left[Z^{ar}_{nm} + Z^a_n \delta_{nm}\right]^{-1} \{Z^{ar}_{n0}\}\right)}{Re(Z^{ar}_{00})} \qquad n,m=1...4$$

(3-1)

Using Equations 2-16, 17, and 18, and canceling the common surface areas S_n, Equation 3-1 can be written as Equation 3-2 in terms of specific acoustic impedances:

$$G_R = \frac{Re\left(z^{ar}_{00} - \{z^{ar}_{mo}\}^T \left[z^{ar}_{nm} + z^a_n \delta_{nm}\right]^{-1} \{z^{ar}_{n0}\}\right)}{Re(z^{ar}_{00})} \qquad n,m=1...4$$

(3-2)

where:

$$z^{ar}_{00} = \rho c \left((ka)^2 + jka\right)$$

$$z^{ar}_{nm} + z^a_n \delta_{nm} = \rho c \left((ka)^2 + jka\right) - j\frac{3\gamma P_0}{c(ka)} \quad \text{when } n=m$$

$$z^{ar}_{nm} + z^a_n \delta_{nm} = z^{ar}_{nm} = \rho c \left((ka)^2 + jka\right)\frac{ka}{kl_{nm}} ej(ka-kl_{nm}) \quad \text{when } n \neq m$$

$$z^{ar}_{n0} = \rho c \left((ka)^2 + jka\right)\frac{ka}{kl_{n0}} ej(ka-kl_{n0})$$

and l_{nm} is the distance between element n and m, the subscript 0 denoting the transducer. Using simple trigonometry, kl_{nm} for $n,m \neq 0$ can be written in terms of m, n, and kl_{n0} as Equation 3-3 for the planar case.

$$kl_{nm} = kl_{n0} \, 2 \sin\left(\frac{\pi}{N}|n-m|\right) \quad \text{where } n,m = 1...N$$

(3-3)

21

Using Equations 3-2 and 3-3, the gain in radiation resistance seen by the transducer, G_R, can be expressed in terms of ka and kl_{no}.

The gain in radiation resistance for the N=4, planar configuration can be plotted in the form of surface and contour plots using Equation 3-1, as shown in Figures 3-2a and 2b. It should be pointed out that here and in all subsequent surface plots of G_R, no spurious peaks were observed, and no smoothing has been applied. Inspection of these graphs reveals two local maxima, one of magnitude 4.34 at ka=0.975 ka_r, kl_{no}=0.5 and another of magnitude 1.79 at ka=1.005 ka_r, kl_{no}=2.7, where ka_r equals 0.01379, the resonance value of ka for a single air filled bubble at one atmosphere ambient pressure. The local maximum at ka=0.975 ka_r, kl_{no}=0.5 is an artifact of the range of kl_{no} chosen. In fact, the gain in radiation resistance diverges as $(kl_{no})^{-1}$ when kl_{no} approaches zero. This case is uninteresting and will not be considered further. The interesting local maximum at ka=1.005 ka_r, kl_{no}=2.7 represents a gain in the radiation resistance seen by the transducer by a factor of almost two. Note that kl = π corresponds to a separation distance of one-half wavelength. A maximum gain in radiation resistance is therefore obtained when the resonators are located a distance just under one-half wavelength from the transducer.

The gain in radiation resistance for the planar configuration where N is set equal to eight and fifteen is shown in Figures 3-2c thru 3-2f. These plots display similar characteristics to the N = 4 case. All

show a local maximum of magnitude approximately two at $ka \cong ka_r = 0.01379$ and $kl_{n0} \cong \pi$.

The local maximum values for G_R at $kl_{n0} \cong \pi$, $ka \cong ka_r = 0.01379$ for various values of N ranging from 2 to 25 and their associated parameters are tabulated in Table 3-1. Two major points can be observed from Table 3-1. First, the resonant bubbles' volume velocity leads the transducer's by a phase shift of approximately 90° (equivalent to -270°). This phase shift is created in two parts. Since the separation between transducer and resonator is approximately one half a wavelength, this introduces a shift of -180° in phase due to simple wave propagation. The remaining -90° is introduced at the surface of a compact resonating bubble between the incident and scattered wave as predicted by Equation 2-24. Second, note that little is gained as one increases the number of resonators beyond about four.

N	G_R	ka_{max}	kl_{max}	$mag(U_n^{rel})$	$arg(U_n^{rel})$
2	1.25	.01386	2.5	.358	83°
4	1.79	.01386	2.7	.546	77°
6	1.95	.01386	2.8	.472	92°
8	1.95	.01386	2.9	.352	88°
10	1.95	.01386	2.9	.284	90°
15	1.94	.01386	2.8	.191	94°
20	1.95	.01379	2.9	.144	93°
25	1.95	.01379	2.8	.113	91°

Table 3-1. Values of G_R for Values of N Ranging from N=2 to 25 and the Parameters Associated with the Local Maximum at $kl_{n0} \cong \pi$, $ka \cong ka_r = 0.01379$ for the Planar Configuration.
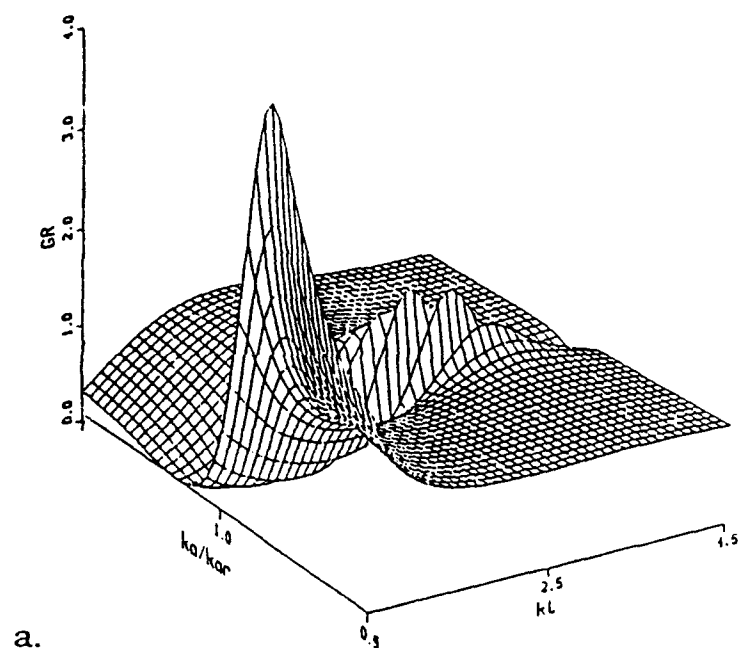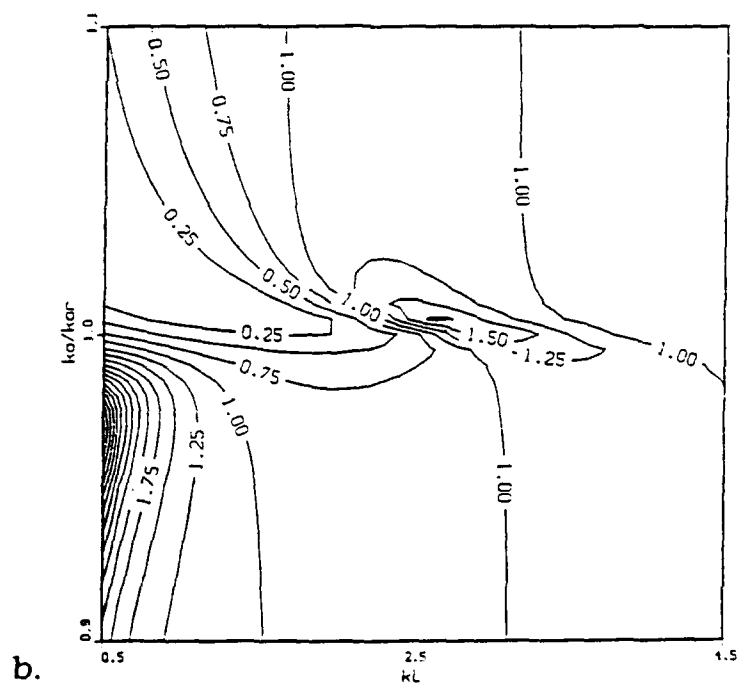
Figure 3-2a,b. Three Dimensional and Contour Plots of G_R as a Function of ka and kl_{no} for N= 4, Planar Configuration, 1 atm.
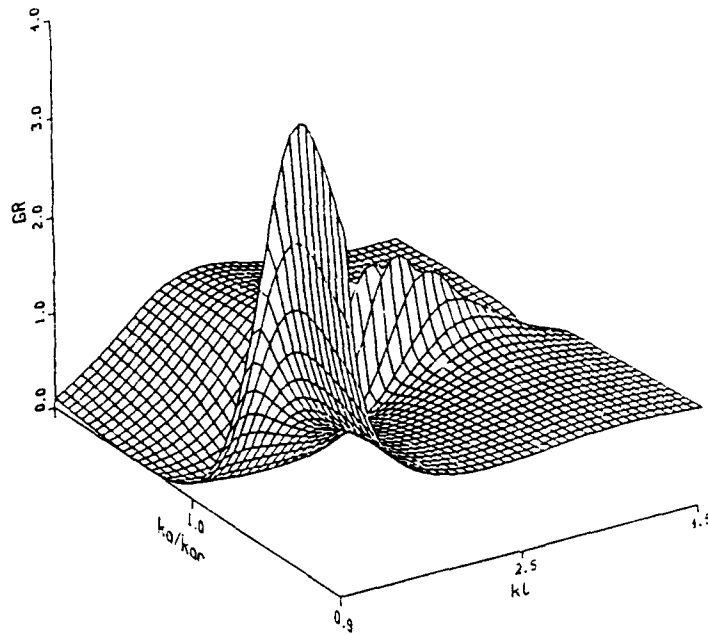
c.
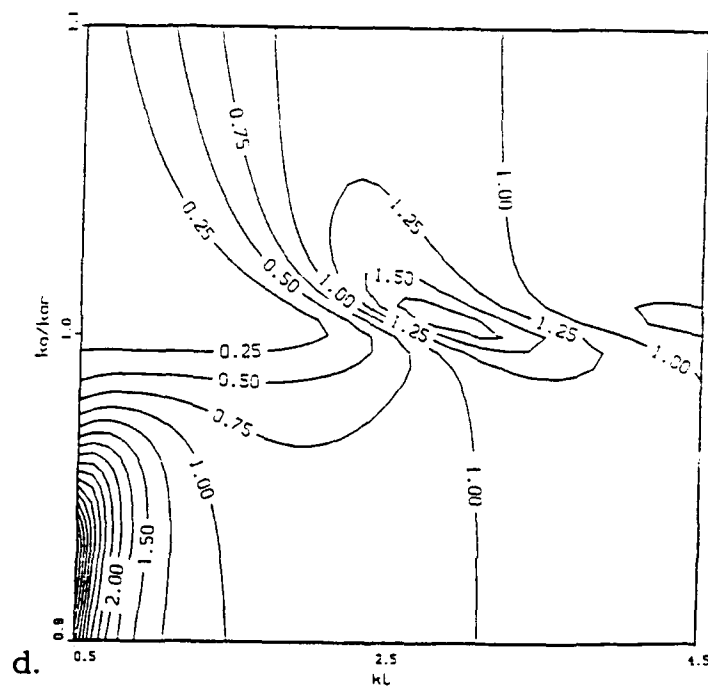
d.

Figure 3-2c,d. Three Dimensional and Contour Plots of G_R as a Function of ka and kl_{no} for N=8, Planar Configuration, 1 atm.

e.
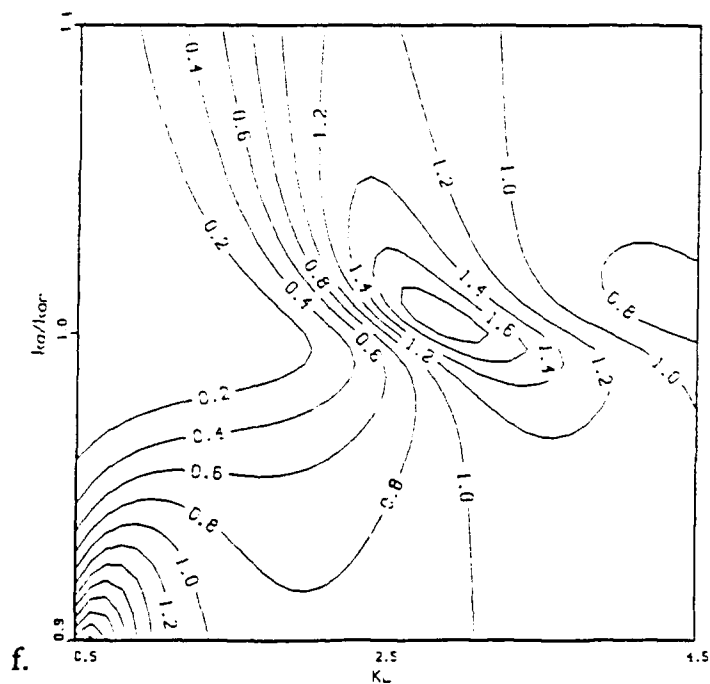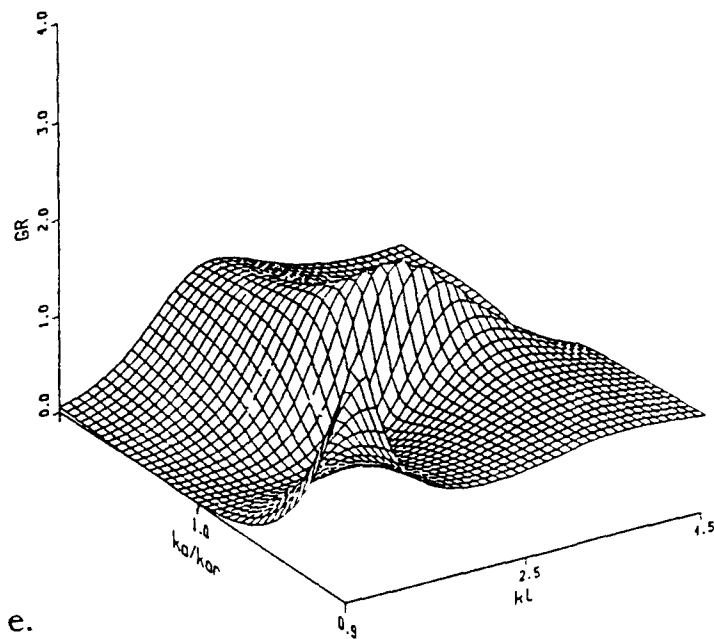

f.

Figure 3-2e,f. Three Dimensional and Contour Plots of G_R as a Function of ka and kl_{n0} for N=15, Planar Configuration, 1 atm.

26

a. PLANAR CONFIGURATION BEAM PATTERN

Polar plots of the beam patterns can be developed for the planar configuration using the axis system defined in Figure 3-3. The origin is located at the transducer, with the resonators located in the x,y plane and θ being the angle measured from the positive y axis in the x,y plane.

Figure 3-4 clearly demonstrates the acoustic advantage of the planar configuration over that of a lone transducer. The zero dB reference is taken as the field of an identical transducer with equal volume velocity in absence of the resonators.
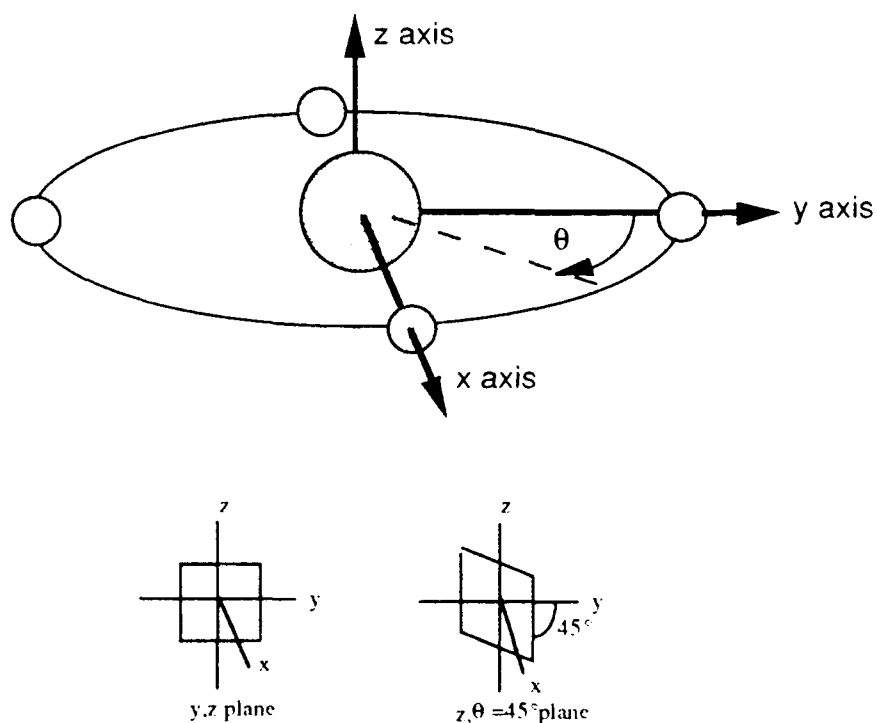
Figure 3-3. Axis System for Beam Patterns Plots, Planar Configuration. Note the definitions of y,z and z, θ=45° Plane

27
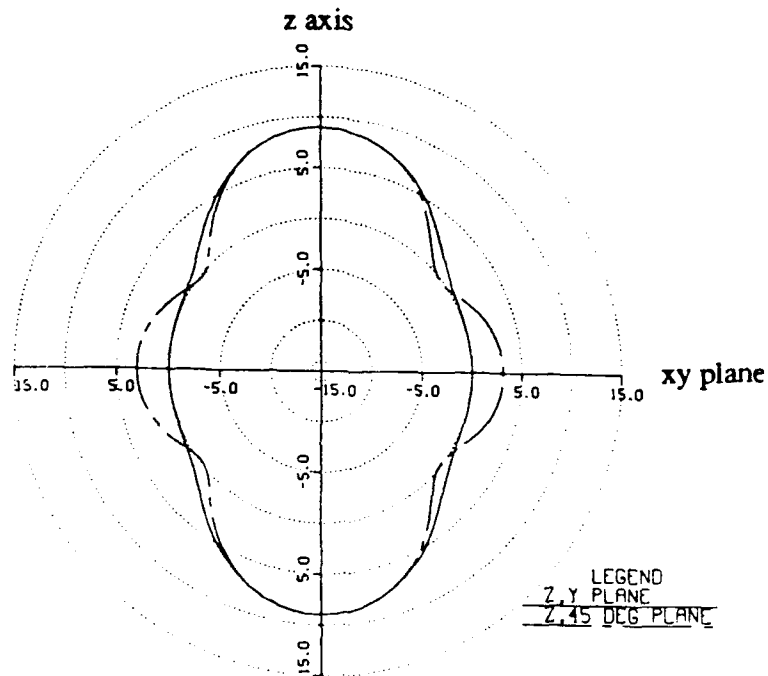
Figure 3-4.   Beam Pattern for the Planar
Configuration in the y,z Plane and the z,θ=45°
Plane, P_0= 1atm. Scale in Decibels (dB).

2. CONICAL CONFIGURATION

The second geometric arrangement analyzed was chosen to take advantage of the 90° phase shift between the volume velocity of the resonators and the transducer for maximum radiated power. If the transducer is offset from the plane of the resonators by one quarter wavelength along the positive z axis, the radiation from the resonators will constructively interfere with that of the transducer along the positive z axis. This configuration will increase the directivity of the system. This arrangement will be referred to as the conical configuration and is shown in Fig. 3-5.
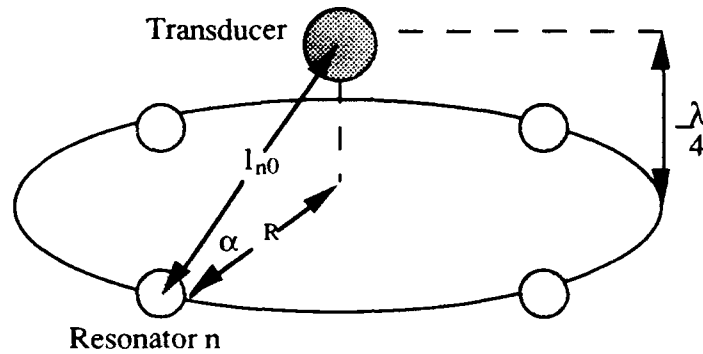
Figure 3-5. Resonators Equally Spaced Around Transducer in a Conical Configuration at Radius R and N = 4. The Transducer is Offset From the Plane of the Resonators by a Distance of $\lambda/4$.

The value of G_R can again be expressed in terms of ka and kl_{n0} using Equation 3-1, where Equation 3-3 is used to express kl_{nm} in terms of n, m, and kl_{n0} for the conical configuration.

$$kl_{nm} = \sqrt{(kl_{n0})^2 - \left(\frac{\pi}{2}\right)^2} \; 2\sin\left(\frac{\pi}{N}|n\text{-}m|\right) \quad \text{where } n,m = 1...N \tag{3-3}$$

The gain in radiation resistance for the conical configuration for the cases N=4, 8 and 15 are plotted in the form of surface and contour plots, as shown in Figures 3-6a through 6f. Inspection of these plots reveals the existence of the same local maximum as the planar configuration of magnitude about 2 at $kl_{n0} \cong \pi$, and ka $\cong$ .01379. Note that, unlike the planar case, the kl axis of Figures 3-6a through f begins at kl_{n0}=1.75 vice 0.5. This is due to the displacement of the transducer in the positive z direction. This displacement requires kl_{n0} be at least $\pi/2$.

The local maximum values for G_R at $kl_{no} \cong \pi$, $ka \cong .01379$ for various values of N ranging from 2 to 25 and their associated parameters are tabulated in Table 3-2 for the conical configuration. In each case the value of G_R for the conical configuration is slightly less than for the planar configuration. Also, the value of kl_{max} is slightly greater for the the conical configuration, but is still approximately equal to π. (A value of π for kl_{no} corresponds to a value of 30 degrees for the angle α in Figure 3-5.)

N	G_R	ka_{max}	kl_{max}	$mag(U_n^{rel})$	$arg(U_n^{rel})$
2	1.27	.01386	2.7	.377	80°
4	1.71	.01386	2.9	.528	78°
6	1.81	.01386	3.1	.421	83°
8	1.82	.01386	3.1	.321	90°
10	1.82	.01386	3.1	.255	90°
15	1.81	.01386	3.1`	.168	82°
20	1.82	.01379	3.1	.128	89°
25	1.82	.01372	3.1	.103	91°

Table 3-2. Values of G_R for Values of N Ranging from N=2 to 25 and the Parameters Associated with the Local Maximum at $kl \cong \pi$, $ka \cong kl_r = 0.01379$ for the Conical Configuration.

a.

b
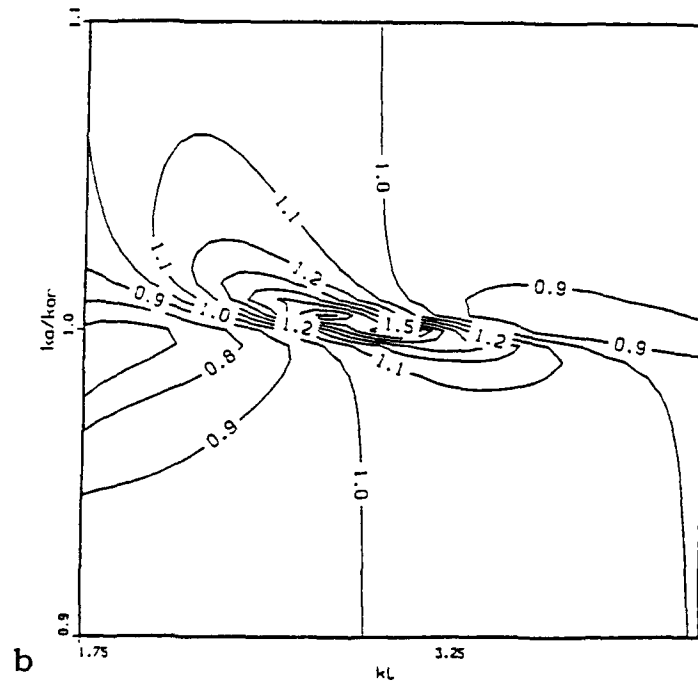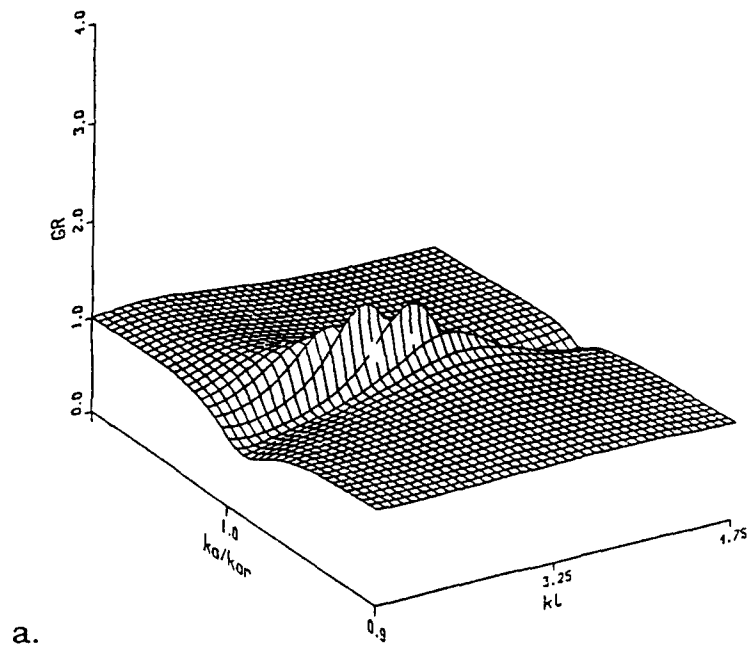
Figure 3-6a,b. Three Dimensional and Contour Plots of G_R as a
Function of ka and kl_{no} for N= 4, Conical Configuration, 1 atm
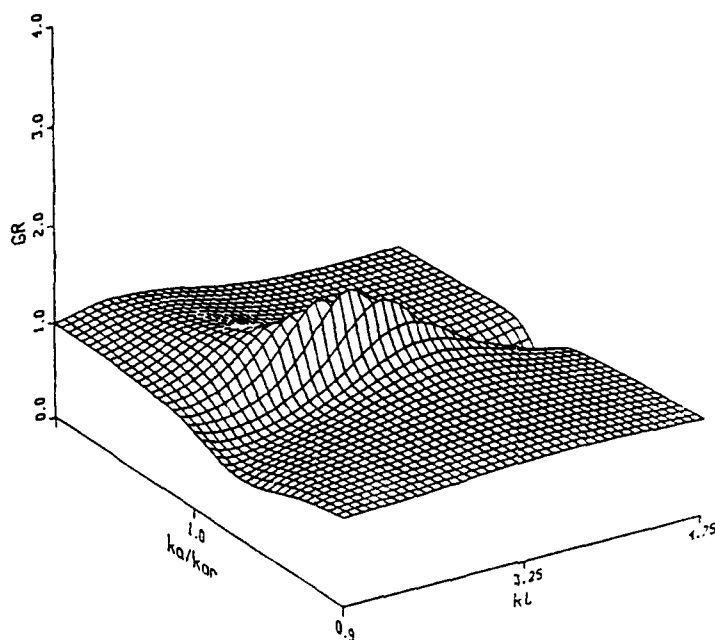
c.
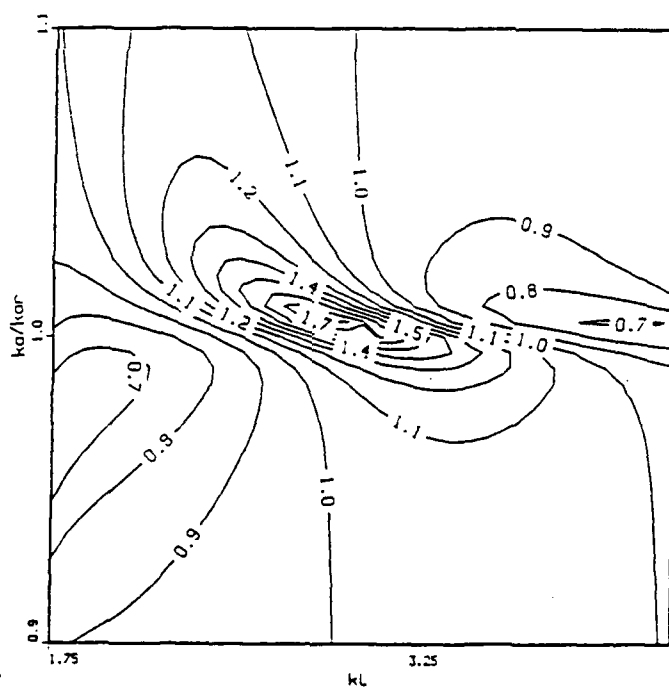
d.

Figure 3-6c,d. Three Dimensional and Contour Plots of G_R as a Function of ka and kl_{no} for N= 8, Conical Configuration, 1 atm.
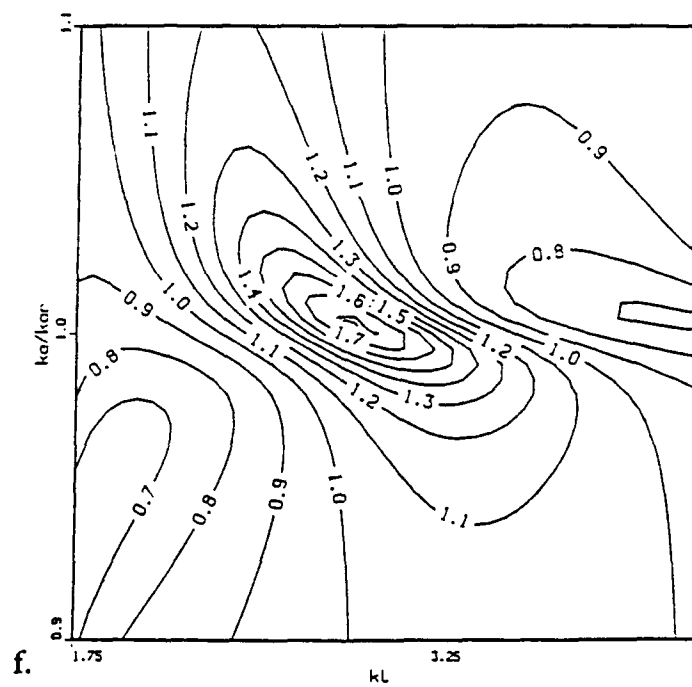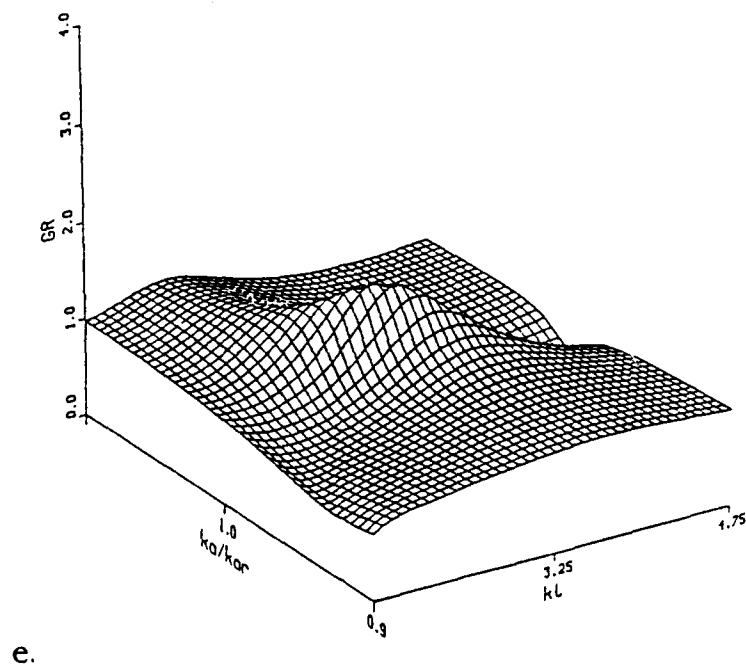
32

e.

f.

Figure 3-6e,f. Three Dimensional and Contour Plots of G_R as a Function of ka and kl_{no} for N=15, Conical Configuration, 1 atm.

33

a. CONICAL CONFIGURATION BEAM PATTERN

To demonstrate the improved directivity of the conical configuration over that of the planar system, polar plots can be developed using the axis system as defined in Figure 3-7, where the transducer is displaced is in the positive z direction from the plane of the resonators.
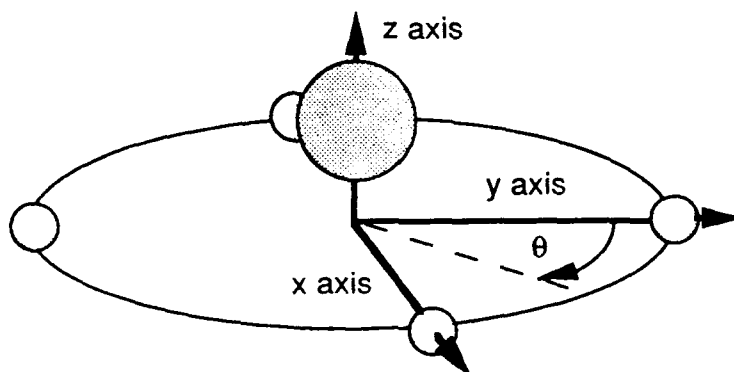
Figure 3-7. Axis System for Beam Pattern Plots, Conical Configuration.

Figure 3-8a shows the beam pattern of the conical configuration in both the y,z and the z,θ=45° plane. As expected, the symmetry in the y,z plane about the z axis is lost, with the sound pressure level (SPL) in the positive z direction being 8 dB greater than in the negative z direction. If one compares the beam pattern of the conical configuration to that of the planar configuration, shown in Figure 3-8b, one observes that the SPL in the positive z direction for the conical configuration is 1 dB greater than for the planar configuration and 10dB greater than for one transducer alone. Figure 3-8b clearly shows

34

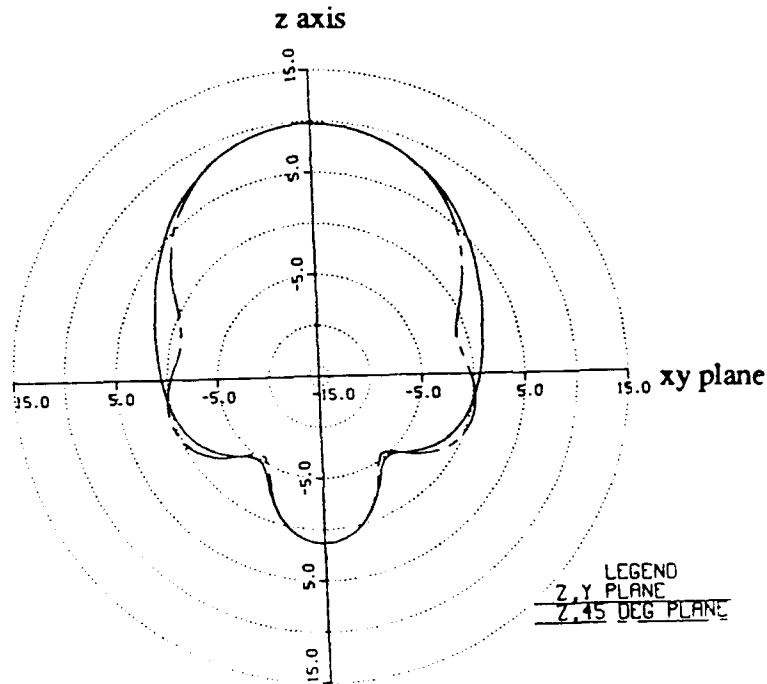that significant directivity can be achieved with only a minor decrease in total power gain, G_R.

z axis

Figure 3-8a. Beam Pattern for the Conical Configuration in the y,z Plane and z,θ=45° Plane, P_0= 1atm. Scale in Decibels (dB).
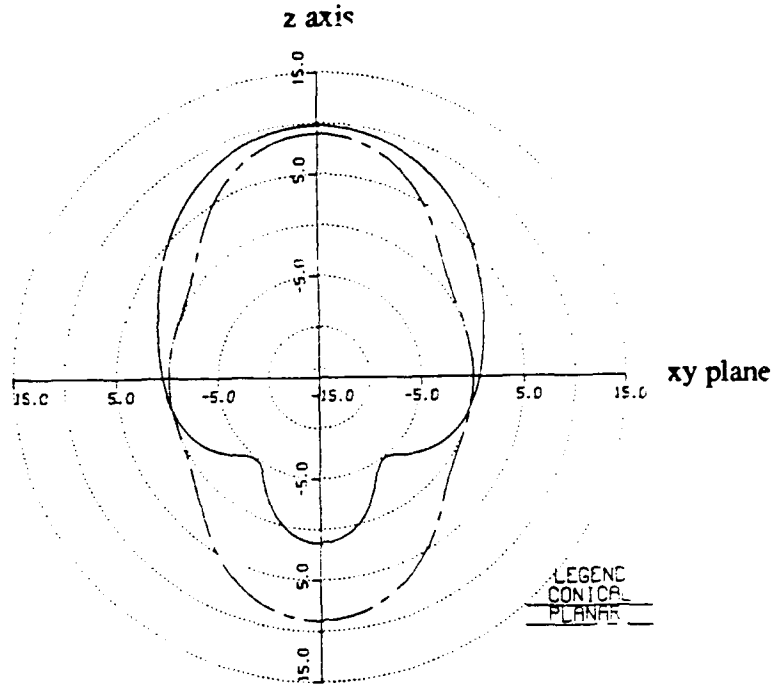
35

z axis

xy plane

Figure 3-8b. Beam Pattern for the Planar and Conical Configuration in the y,z Plane, P_0= 1atm. Scale in Decibels (dB).

3. CONFIGURATION DIMENSIONS

The results of all calculations performed have been presented in terms of the dimensionless radius and spacing, ka and kl_{n0}. The actual dimensions for the radius a and the separation distance l_{max} for a given frequency are obtained using Equation 3-4.

$$a = \frac{ka\, c}{2\pi\, f} \qquad\qquad l_{n0} = \frac{kl_{n0}\, c}{2\pi\, f} \qquad\qquad (3\text{-}4)$$

Taking ka $\cong$ ka_r = 0.01379 and kl_{n0} $\cong$ π for the optimum values of a typical system at an ambient pressure of one atmosphere in Equation 3-4, a plot of the resulting dimensions a and l_{n0} as a function of frequency can be made, as shown in Figures 3-9a and 3-9b.

36
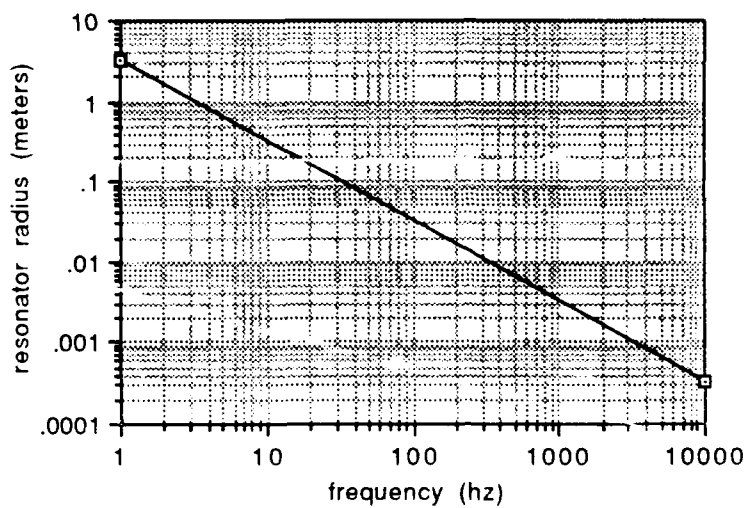
Figure 3-9a. Optimum Resonator Diameter (a) at
Resonance Versus Frequency for a System at $P_0 = 1 atm$.

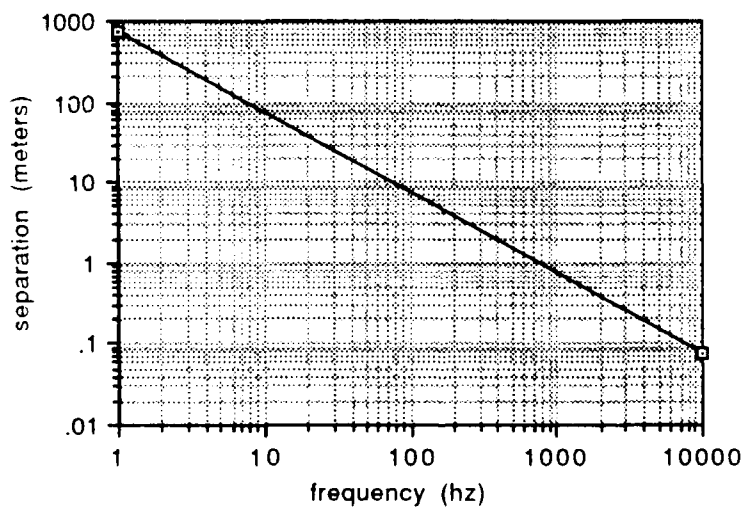Figure 3-9b. Optimum Resonator-Transducer Separation
(l_{no}) Versus Frequency for Maximum Power Gain.

B. ANALYSIS WITH CONSTANT TRANSDUCER ka, AT 50 ATMOSPHERES

Two major assumptions that have been made throughout the analysis up this point need to now be modified. The first is that the ambient pressure is one atmosphere and the second is that the radius of the transducer equals that of the resonators ($ka_0 = ka_n$). In the following analysis, an ambient pressure of 50 atmospheres (corresponding to a depth of 500 meters) will be taken as a more realistic value for an operational system. Since the internal acoustic impedance of a bubble is a function of depth, the value for ka_r of a single bubble at resonance will shift from 0.01379 ($P_0 = 1atm$) to 0.09754 ($P_0 = 50atm$). Also, the value of ka_0 will no longer be considered equal to that of the resonators, but will be held constant at various specific values.

In the previous sections it was shown that little is gained when the number of sympathetic resonators is greater than about four; hence the following analysis will be restricted to the case N=4. Conducting similar calculations as before, contour plots and surface plots have been generated for the cases N = 4, ka_0 = 0.05, 0.10 and 0.20, for both the conical configuration (Figures 3-10a through 3-10f) and the planar configuration (Figures 3-11a through 3-11f). As in the previous analyses where the ambient pressure was taken to be one atmosphere, all cases display a local maximum of G_R of almost 2 at around $ka \cong ka_r$ = 0.09754 and $kl \cong \pi$. These maximum values are tabulated in Table 3-3. Also tabulated, though not plotted, are the cases ka_0 = 0.025 and 0.150. The first entry in table 3-3 for either configuration was

38

calculated holding ka_0 equal to ka_n, as in previous calculations, vice holding ka_0 constant. A review of Table 3-3 and Figures 3-11 and 12 demonstrates that the value of ka_0 has little effect on the achievable power gain.

configuration	ka_0	G_R	ka_{max}	kl_{max}	$mag(U_n^{rel})$	$arg(U_n^{rel})$
planar	ka_n	1.89	.09998	2.8	0.657	90°
	.025	1.88	.09998	2.8	0.041	90°
	.050	1.88	.09998	2.8	0.165	90°
	.100	1.89	.09998	2.8	0.657	90°
	.150	1.89	.09998	2.8	1.469	90°
	.200	1.89	.09998	2.8	2.590	90°
conical	ka_n	1.78	.09901	3.1	0.607	95°
	.025	1.78	.09950	3.1	0.038	95°
	.050	1.78	.09950	3.1	0.154	95°
	.100	1.78	.09950	3.1	0.613	95°
	.150	1.79	.09950	3.1	1.376	95°
	.200	1.79	.09950	3.1	2.425	95°

Table 3-3. Values of G_R for Various Values of ka_0 Ranging from .025 to .2 and the Parameters Associated with the Local Maximum at $kl \cong \pi$, $ka \cong ka_r = 0$ 0.09754 for both the Conical and Planar Configurations at $P_0 = 50$atm.
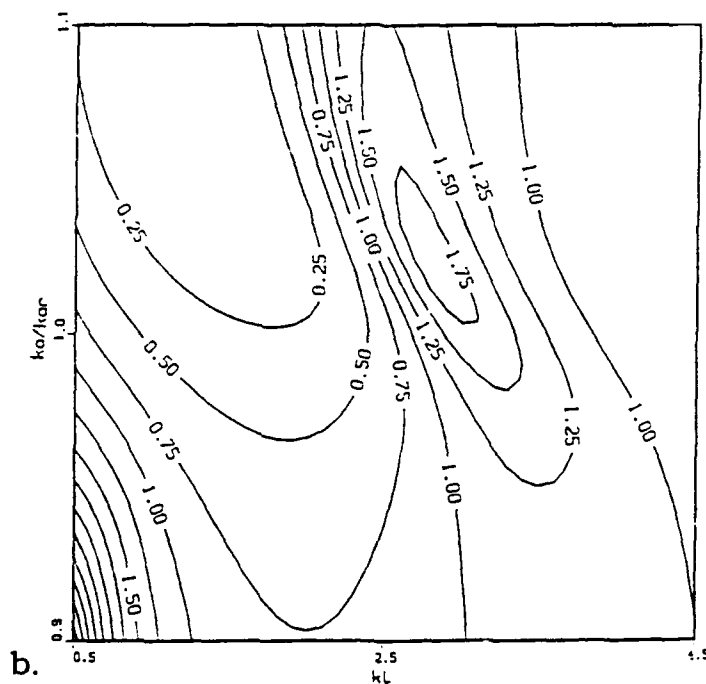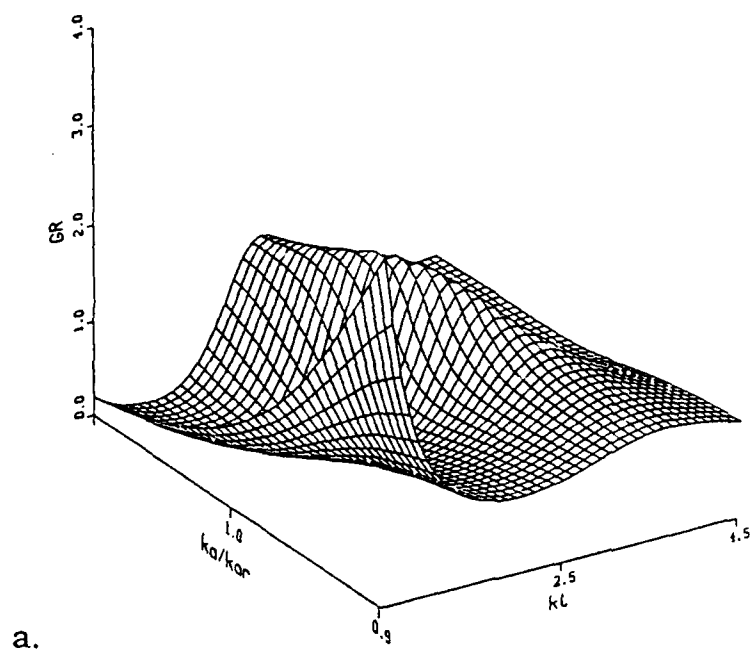
Figure 3-10a,b. Three Dimensional and Contour Plots of G_R as a Function of ka and kl_{n0} for N= 4, Planar Configuration, 50 atm. ka_0 = 0.05.
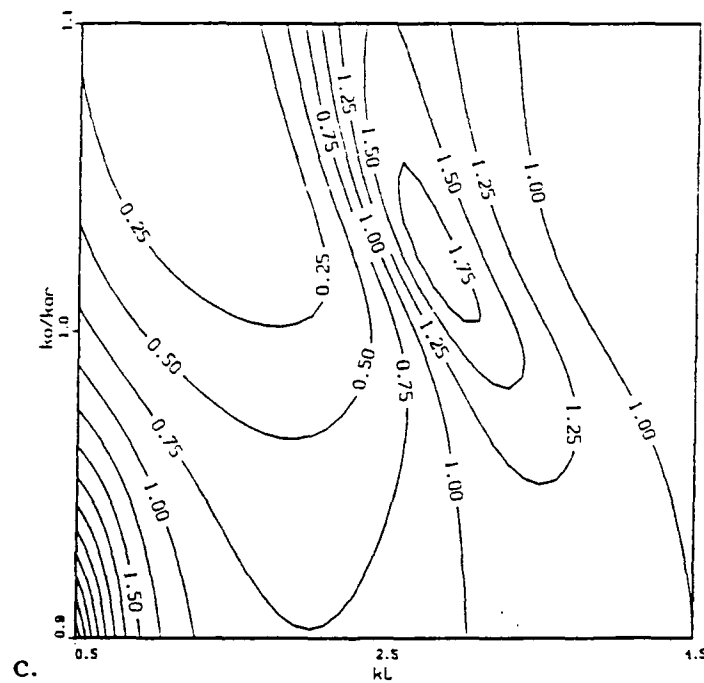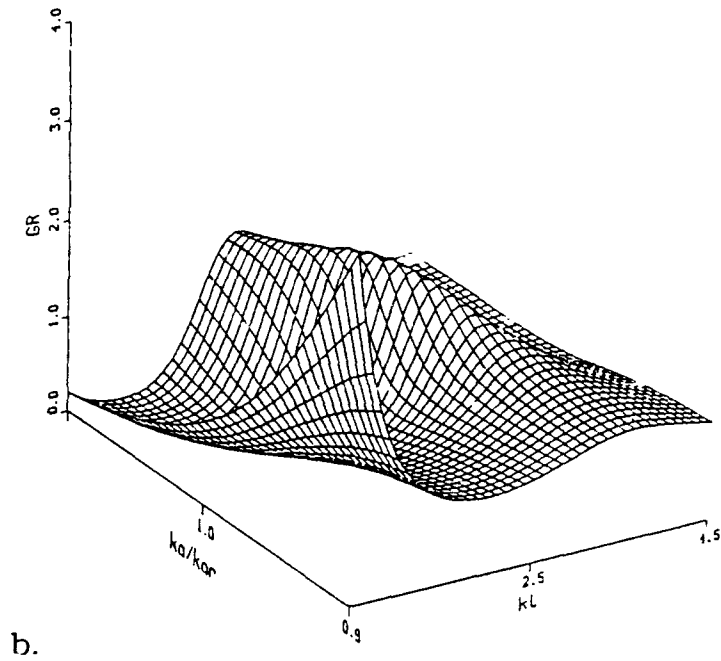
b.

c.

Figure 3-10c,d. Three Dimensional and Contour Plots of G_R as a Function of ka and kl_{no} for N= 4, Planar Configuration, 50 atm. $ka_0 = 0.10$.

41

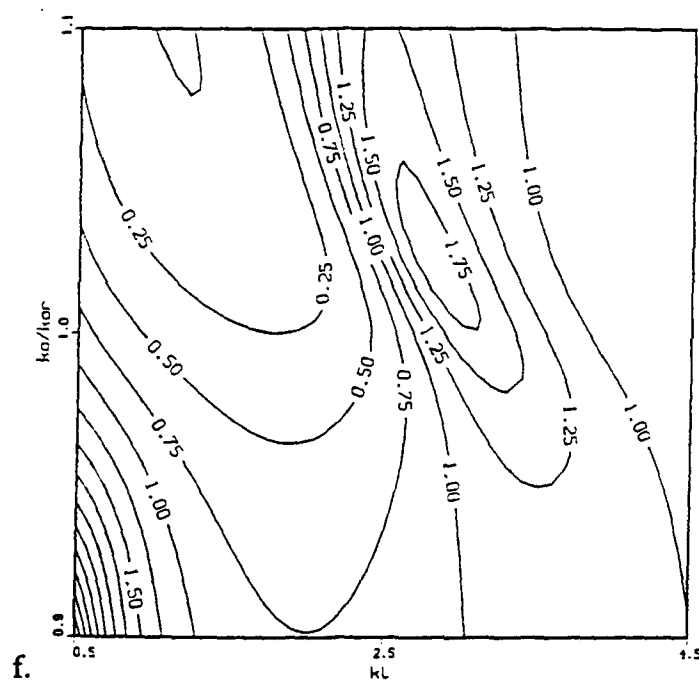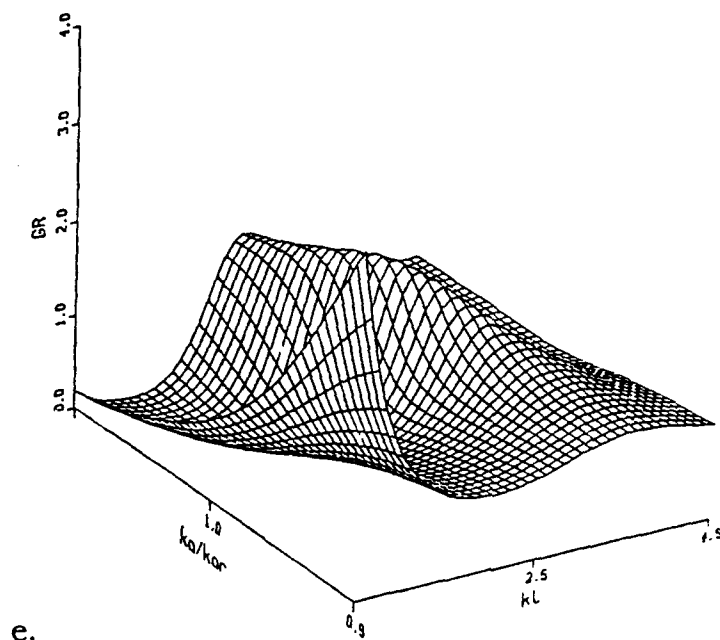e.

f.

Figure 3-10e,f. Three Dimensional and Contour Plots of G_R as a
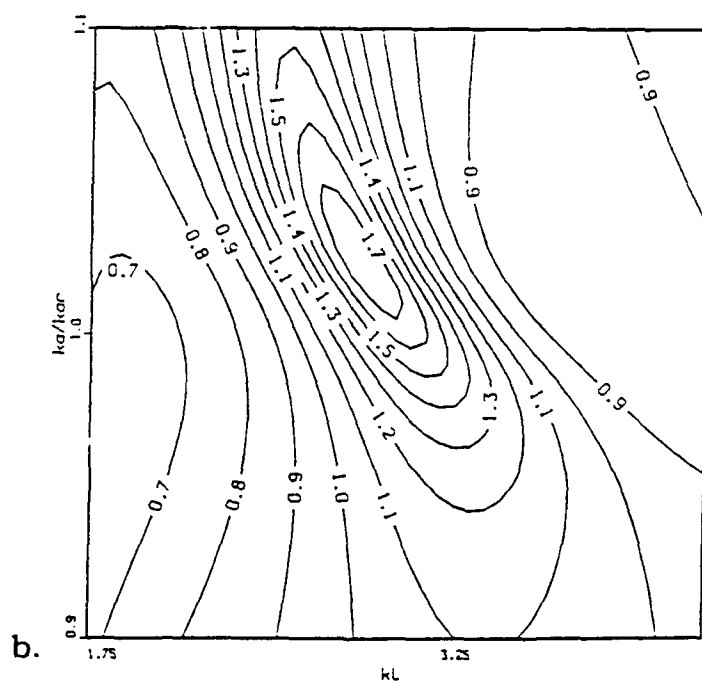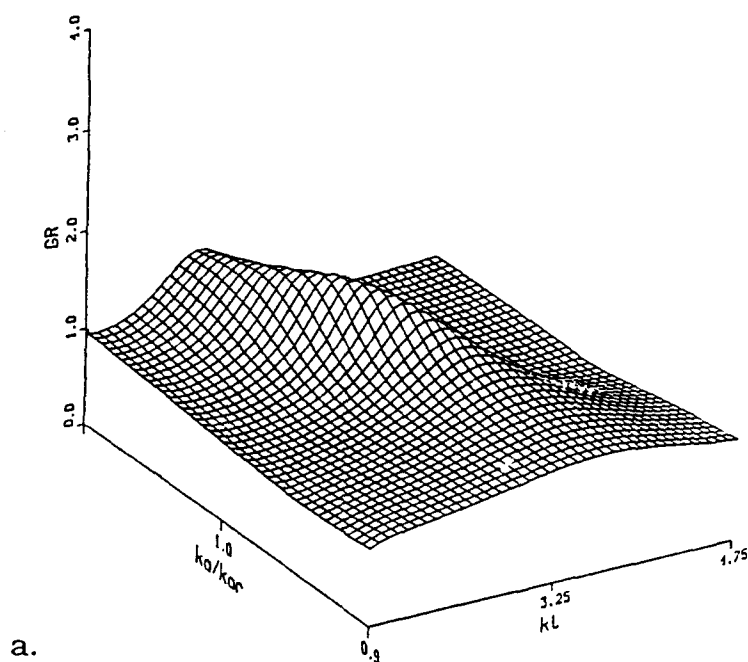Function of ka and kl_{no} for N= 4, Planar Configuration, 50 atm.
ka_0 = 0.20.

Figure 3-11a,b. Three Dimensional and Contour Plots of G_R as a Function of ka and kl_{no} for N= 4, Conical Configuration, 50 atm. ka_0 = 0.05.

c.

d.

Figure 3-11c,d. Three Dimensional and Contour Plots of G_R as a Function of ka and kl_{n0} for N= 4, Conical Configuration, 50 atm. ka_0 = 0.10.

44

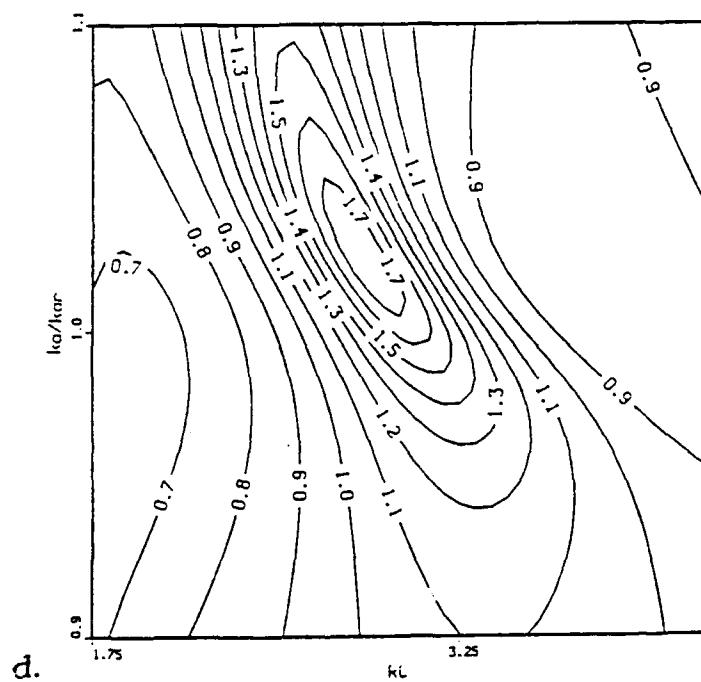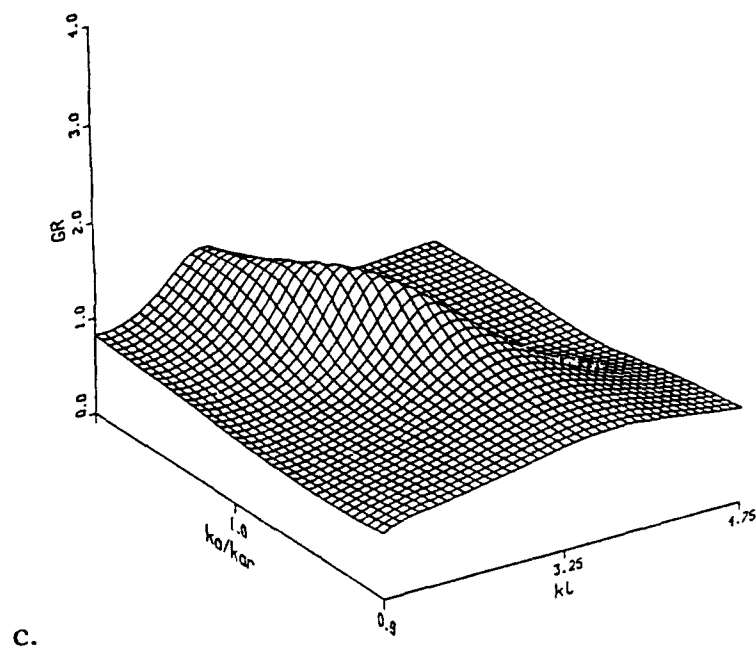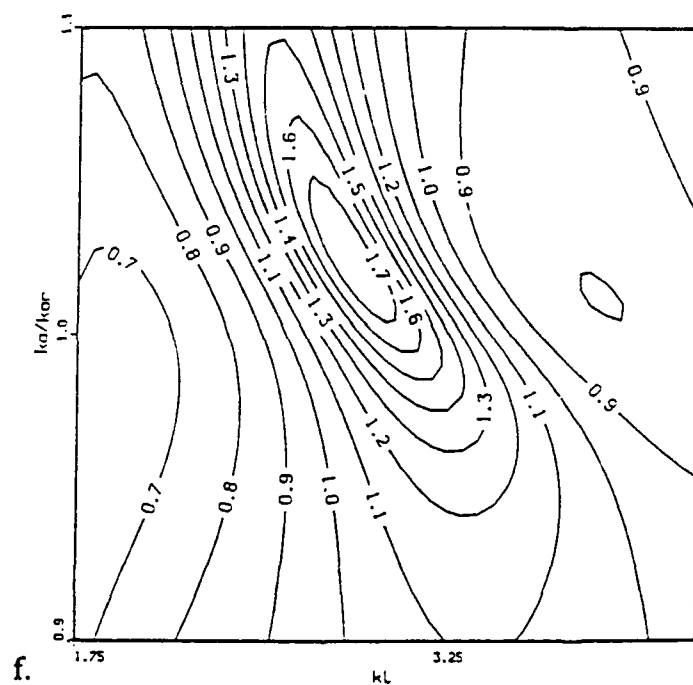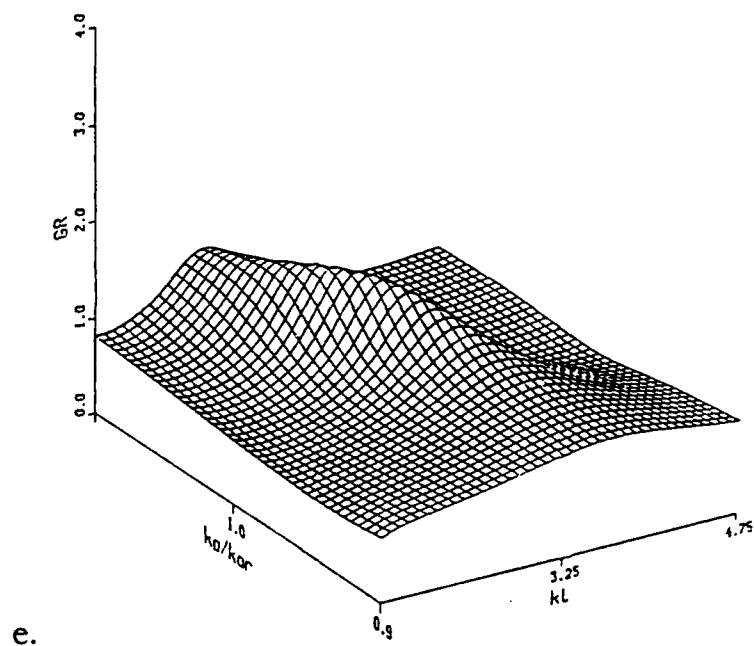e.

f.

Figure 3-11e,f. Three Dimensional and Contour Plots of G_R as a Function of ka and kl_{n0} for N=15, Conical Configuration, 50 atm. $ka_0 = 0.20$.

45

1. BEAM PATTERNS AT 50 ATMOSPHERES

Since there is no significant variation in gain with the value of ka_0, beam patterns were only developed for the case $ka_0 = ka_r$, shown in Figures 3-12 through 3-14. These plots show the maximum SPL in the positive z direction for the conical configuration to be 1.5 dB greater than for the planar case and 10.5 dB greater than for the transducer in absence of the resonators.

2. CONFIGURATION DIMENSIONS, FIFTY ATMOSPHERES

The actual dimensions of the resonator radius a and the separation distances l_{n0}, for a system operated at an ambient pressure of 50 atmospheres were calculated using Equation 3-4 Using the optimum value $ka \cong ka_r = 0.09754$ and $kl_{n0} \cong \pi$. Since the values of l_{n0} are not depth dependent, Figure 3-9b still applies. Figure 3-15 displays the relation between optimum resonator radius and frequency at 50 atmospheres.
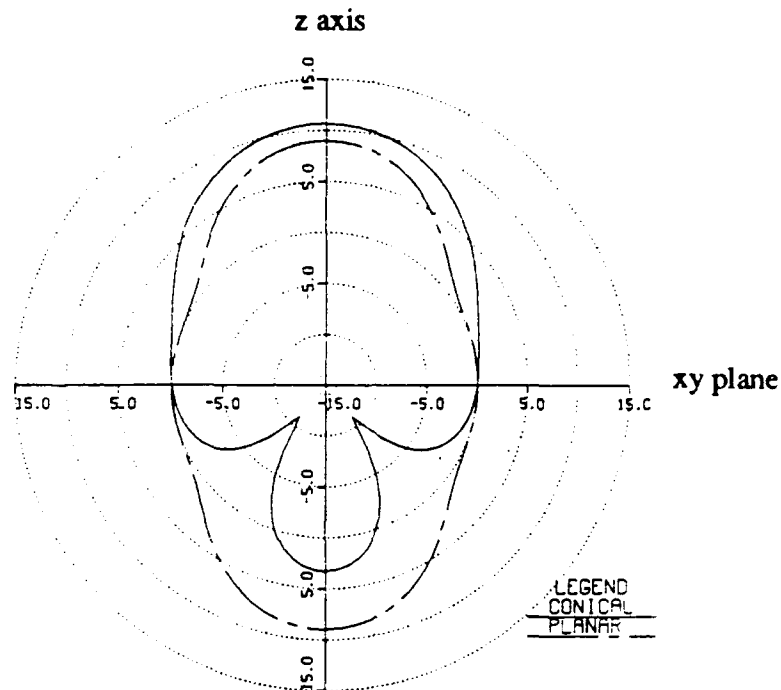
z axis

Figure 3-12. Beam Pattern for Planar and Conical Configuration in the y,z Plane, P_0= 50atm. Scale in Decibels (dB).

z axis
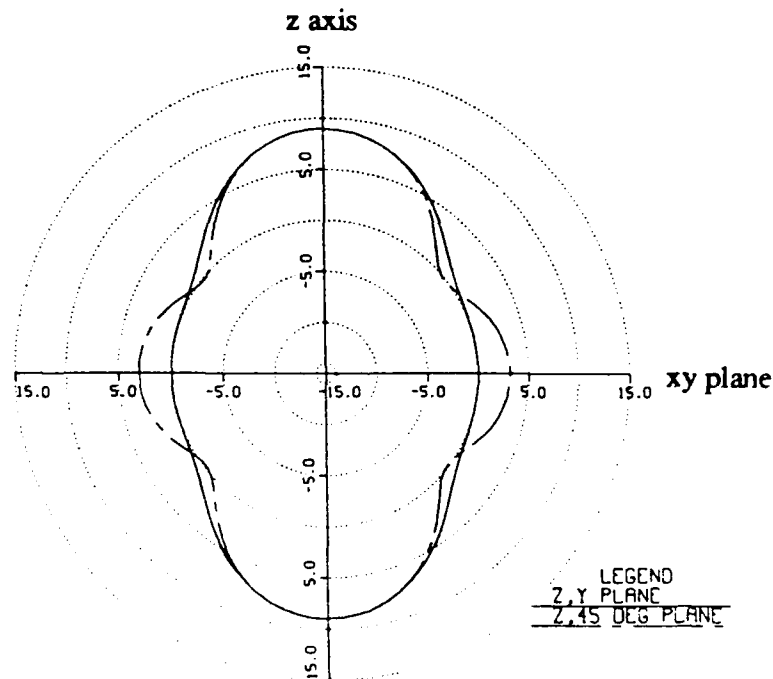
Figure 3-13. Beam Pattern for Planar Configuration in the y,z Plane and z,θ=45° Plane, P_0= 50atm. Scale in Decibels (dB)
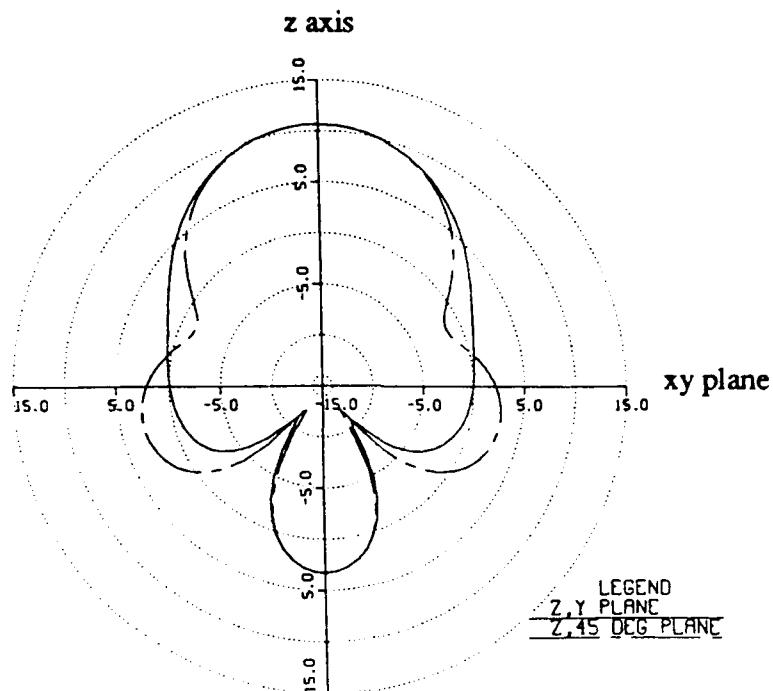
47

z axis

xy plane

LEGEND
Z,Y PLANE
Z,45 DEG PLANE

Figure 3-13. Beam Pattern for Conical
Configuration in the y,z Plane,and z,θ=45°
Plane, P_0= 50atm. Scale in Decibels (dB).
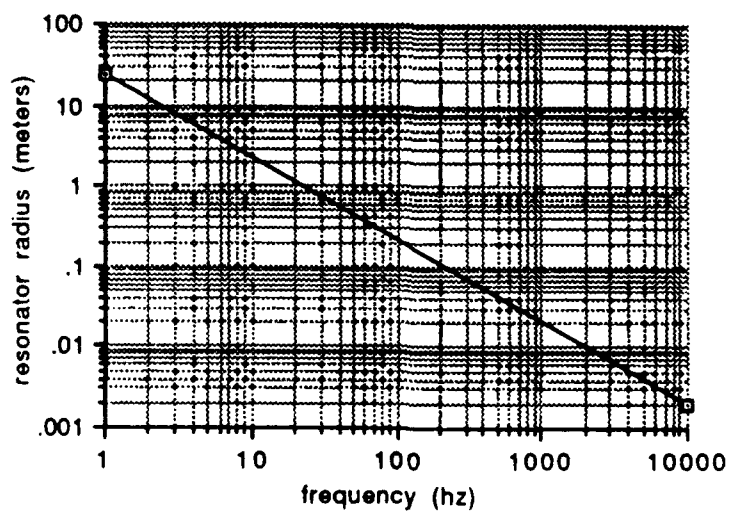

Fig. 3-15. Optimum Resonator Diameter (a) at Resonance
Verses Frequency for a System at P_0= 50atm.

48

IV. SUMMARY, CONCLUSIONS AND RECOMMENDATIONS

A. SUMMARY

The problem of multiple scattering of an incident plane wave from a system of compact resonant scatterers was solved using both Tolstoy's method and network analysis. It was shown that these two methods of analysis are equivalent and that both predict the existence of "quasiresonance". Network analysis was then applied to a circular array of scatterers, where the incident plane wave was replaced by spherical waves radiated from an active transducer, located on the axis center. The acoustic advantage of this system was quantified by the gain in the radiation resistance seen by the transducer in the presence of these scatterers compared to a lone transducer. Two configurations were analyzed, (1) the transducer in the plane of the resonators and (2) the transducer displaced by one-quarter wavelength from the plane. Both configurations showed a gain in radiation resistance of almost a factor of two and improved directivity over that of a single transducer.

B. CONCLUSIONS

The numerical analysis of a transducer surrounded by a circular array of sympathetic resonators indicates that a gain in radiation resistance of about two is obtainable compared to a lone transducer. The physical dimensions of such a system operating at an ambient

49

pressure of 50 atmospheres are displayed in Table 4-1 for several frequencies of interest.

Frequency (Hz)	Resonator Radius (a) (m)	System Radius (R) (m)	
		conical	planer
10	0.329	64.9	74.9
100	0.0329	6.49	7.49
1000	0.00329	0.649	0.749

Table 4-1. Dimensions of Planer and Conical Configurations for Various Frequencies, P_o = 50 atm., R is the radius of the array.

Although the calculations presented here were for spherical bubbles, the results also apply to more realistic devices (e.g.thin shelled cavities, balloons, etc) as long as they are compact (ka<<1). M. Strasberg [Ref. 7] showed that the shape of a resonant body has little effect on its fundamental resonance frequency. For example, he calculated that an oblate spheroid with a ratio of lengths of major to minor axes of four, the fundamental resonance frequency differs by only a factor of 1.08 from that of a sphere with the same volume. Therefore, any deformation of the resonators from a true spherical shape, for example due to forces such as buoyancy, should have little affect on system performance.

C. RECOMMENDATIONS

The results of the research reported in this thesis are very encouraging. It is recommended that follow-on work include the

design, construction, and testing of an array to verify the theoretical predictions presented.

Theoretical analysis remains to be conducted in at least four areas. First, in all of the calculations performed, the sympathetic resonators were assumed to be gas-filled air bubbles executing radial oscillations only. A more realistic model of a sympathetic resonator may be required, based upon the properties of a practical device. It is recommended this be investigated. Second, Tolstoy has shown that the scattering of an incident plane wave from a linear array of resonant scatterers exhibits strong directionality. Perhaps a linear array of sympathetic resonators offers better performance gain than the circular arrays considered in this research. It is recommended that such a configuration be investigated. Third, it was shown that in the optimum conical configuration the ring of sympathetic resonators lies on a cone with a apex angle of approximately 120 degrees, independent of frequency. This suggests that a broad-band, constant directivity system could be constructed using a series of concentric rings of resonators, each tuned to a slightly different frequency and placed in its appropriate location along the surface of such a cone, as indicated in Figure 4-1. It is recommended that the properties of such a system be investigated. Fourth, in the calculations presented, the sympathetic resonators were all assumed to be identical, and their locations were assumed to be precisely known, as well as that of the transducer. It is recommended that the effects of resonator nonuniformity and imprecise location be investigated.
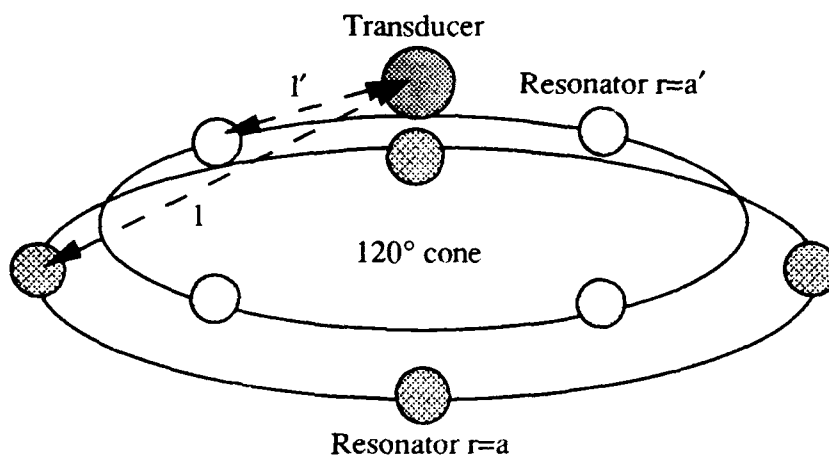
Transducer

l′

Resonator r=a′

120° cone

Resonator r=a

Figure 4-1. Conical Geometric Configuration Allowing an Expanded Frequency Response Using Two Concentric Rings of Resonators of Radius a and a', at a Separation Distance from the Transducer of l and l'.

APPENDIX

PROGRAMING INFORMATION

Inquires into the computer programs used to develop the system

parameters and associated graphics should be addressed to:

Professor S.R. Baker
Physics Department, Code BA
Naval Postgraduate School
Monterey, California 93943
Tel. (408) 646-2732/2729
Autovon 878-2732/2729

REFERENCES

[1] Tolstoy, I., "Superresonant Systems of Scatterers. I,"*Journal of the Acoustical Society of America,* **80**(1), pp. 282-294, 1986.

[2] Tolstoy, I., "Erratum: Superresonant Systems of Scatterers. I,"*Journal of the Acoustical Society of America,* **81**(6), pp. 282-294, 1986.

[3] Tolstoy, A. and Tolstoy I., "Superresonant Systems of Scatterers. II,"*Journal of the Acoustical Society of America,* **83**(6), pp. 2086-2096, 1988.

[4] Tolstoy, I., "Resonance and Directionality of Linear Arrays of Monopole Scatterers.,"*Journal of the Acoustical Society of America,* Suppl. 1, **84**, pp. S218, 1988.

[5] Lighthill, J. M., *Waves in Fluids,* pp. 19,53, Cambridge University Press, 1978.

[6] Kinsler, L. E., Frey, A. R., Coppens, A. B., and Sanders, J. V., *Fundamentals of Acoustics,* pp. 228-231 John Wiley & Sons, Inc., 1982.

[7] Strasberg, M., "The Pulsation Frequency of Nonspherical Gas Bubbles in Liquids,"*Journal of the Acoustical Society of America.* v. 25(3), pp. 536-537, 1953.